

---

This is an electronic reprint of the original article.  
This reprint may differ from the original in pagination and typographic detail.

Kaario, Ossi Tapani; Karimkashi, Shervin; Bhattacharya, Atmadeep; Vuorinen, Ville; Larmi, Martti; Bai, Xue Song

## A comparative study on methanol and n-dodecane spray flames using Large-Eddy Simulation

*Published in:*  
Combustion and Flame

*DOI:*  
[10.1016/j.combustflame.2023.113277](https://doi.org/10.1016/j.combustflame.2023.113277)

Published: 01/02/2024

*Document Version*  
Publisher's PDF, also known as Version of record

*Published under the following license:*  
CC BY

*Please cite the original version:*  
Kaario, O. T., Karimkashi, S., Bhattacharya, A., Vuorinen, V., Larmi, M., & Bai, X. S. (2024). A comparative study on methanol and n-dodecane spray flames using Large-Eddy Simulation. *Combustion and Flame*, 260, Article 113277. <https://doi.org/10.1016/j.combustflame.2023.113277>

---

This material is protected by copyright and other intellectual property rights, and duplication or sale of all or part of any of the repository collections is not permitted, except that material may be duplicated by you for your research use or educational purposes in electronic or print form. You must obtain permission for any other use. Electronic or print copies may not be offered, whether for sale or otherwise to anyone who is not an authorised user.



# A comparative study on methanol and *n*-dodecane spray flames using Large-Eddy Simulation

Ossi Tapani Kaario<sup>a,\*</sup>, Shervin Karimkashi<sup>a</sup>, Atmadeep Bhattacharya<sup>a</sup>, Ville Vuorinen<sup>a</sup>, Martti Larmi<sup>a</sup>, Xue-Song Bai<sup>b</sup>

<sup>a</sup> Aalto University, School of Engineering, Department of Mechanical Engineering, 00076 Aalto, Finland

<sup>b</sup> Lund University, Lund, Sweden

## ARTICLE INFO

### Keywords:

LES  
methanol  
*n*-dodecane  
spray  
Chemistry  
combustion  
3D  
0D

## ABSTRACT

Methanol (CH<sub>3</sub>OH) is an attractive alternative fuel that can reduce net carbon release and decrease pollutant emissions. In this study, methanol and *n*-dodecane spray flames were investigated using Large-Eddy Simulation (LES) and direct coupling with finite-rate chemistry. The selected ambient conditions are relevant to engines and were previously unreported for numerical methanol spray studies, i.e. high pressure (60 bar) and temperature (900 – 1200 K) with high injection pressure (1500 bar). The Engine Combustion Network (ECN) Spray A case was used to validate the *n*-dodecane spray flame. For methanol, a modified ECN Spray A condition was used with a high initial ambient temperature (1100 K–1200 K) to ensure fast enough ignition relevant to engine time scales. The performed homogeneous reactor (0D) simulations revealed a new phenomenon of a two-stage ignition process for methanol, confirmed by the 3D LES at high pressure, high temperature, and lean conditions. The present numerical results also show that: 1) there is a strong ambient temperature sensitivity for methanol ignition delay time (IDT) with a five-fold decrease in IDT ( $IDT_{1100K}/IDT_{1200K} = 5$ ) and a factor of 2.6 decrease in the flame lift-off length ( $FLOL_{1100K}/FLOL_{1200K} = 2.6$ ) as the ambient temperature is increased from 1100 K to 1200 K, 2) methanol spray ignition takes place at a very lean mixture ( $\phi_{MR} \approx 0.2$ ) consistent with the 0D predicted most reactive mixture fraction ( $Z_{MR}$ ), 3) on average, methanol sprays are significantly leaner than *n*-dodecane sprays at quasi-steady-state ( $\phi_{meoh, ave} \approx 0.2$  vs  $\phi_{ndod, ave} \approx 0.7$ ), implying very low soot emissions, and 4) the methanol spray flames could have similar temperatures as the *n*-dodecane sprays depending on the initial conditions, thus a similar level of NO<sub>x</sub> emissions.

## 1. Introduction

Hydrogen (H<sub>2</sub>), green ammonia (NH<sub>3</sub>), methane (CH<sub>4</sub>), and methanol (CH<sub>3</sub>OH) are considered to be among the key fuels with small molecular structures when targeting hydrogen economies [1]. Methanol is a fuel of high interest as it can be produced carbon-neutrally using recycled CO<sub>2</sub> and green H<sub>2</sub> [2]. In addition, methanol has an oxygen atom in the molecule, which results in low particulate emissions. Furthermore, the infrastructure for methanol production, transportation, and usage mostly exists, making the application of methanol feasible, especially for non-road and marine sectors [2]. On the other hand, there are particular challenges related to methanol use especially considering the low cetane number and the high heat of vaporization (HoV). In the present study, we investigate methanol and *n*-dodecane spray combustion using Large-Eddy Simulation (LES) and direct

chemistry (DC). We start by simulating the Engine Combustion Network (ECN) Spray A for *n*-dodecane [3]. The ECN Spray A resembles engine-like conditions with high injection pressure ( $P_{inj} = 1500$  bar), high gas density ( $\rho_{gas} = 22.8$  kg/m<sup>3</sup>), and temperature ( $T = 900$  K). We then compare reacting methanol sprays in modified Spray A conditions to the *n*-dodecane results, to identify the advantages and shortfalls of methanol as an engine fuel.

Several authors have reported numerical studies on methanol spray combustion. Wang et al. [4] performed LES study of methanol sprays in a pressure swirl atomizer with air co-flow. Low injection pressure was used for methanol, and the LES study focused on developing a turbulent combustion model (FSM) accounting for single droplet combustion while using a global single-step chemistry. The droplet modeling and temperature predictions were well in line with the experiments. Prasad

\* Corresponding author.

E-mail address: [ossi.kaario@aalto.fi](mailto:ossi.kaario@aalto.fi) (O.T. Kaario).

<https://doi.org/10.1016/j.combustflame.2023.113277>

Received 24 May 2023; Received in revised form 19 December 2023; Accepted 20 December 2023

Available online 27 December 2023

0010-2180/© 2023 The Author(s). Published by Elsevier Inc. on behalf of The Combustion Institute. This is an open access article under the CC BY license (<http://creativecommons.org/licenses/by/4.0/>).

et al. [5] used LES of methanol sprays in a vitiated co-flow burner. They used Eulerian stochastic field method and 18 species chemical mechanism and reported a reasonably accurate prediction for different methanol loadings. Jones et al. [6] studied methanol sprays in a pressure swirl atomizer (Simplex atomizer) with air co-flow, where an ultrasonic atomizer produced liquid droplets with low velocity. They also used an Eulerian stochastic field method and an 18-species chemical mechanism with relatively good prediction of velocity and flame lift-off statistics compared to experiments. Furthermore, Sharma et al. [7] studied methanol sprays in the Sydney burner with H<sub>2</sub>-air co-flow using multiple mapping conditioning and LES (MMC-LES) together with a 32-species mechanism. To summarize, several methanol LES spray studies have been carried out using low injection pressure conditions in various burner configurations. To the best of our knowledge, single-fuel high-injection pressure methanol LES investigations are however scarce or non-existent.

Methanol has been used together with high-reactivity fuels such as *n*-dodecane in combustion systems. Considering methanol-related dual-fuel (DF) studies, Karimkashi et al. [8] explored methanol-*n*-dodecane DF ignition in a lean methanol/air and in a lean methane/air mixture under the ECN Spray A conditions using LES and DC. Various ambient temperatures were considered for both DF mixtures. The main conclusion was that the ignition window for *n*-dodecane/methanol DF spray is very narrow compared to the *n*-dodecane/methane mixture. Xu et al. [9] studied the DF ignition characteristics of *n*-heptane spray in a lean methanol mixtures using LES and transported probability density function (TPDF) model coupled with DC. At the ambient temperature of 900 K, they noted long ignition delay times (IDT) and a strong equivalence ratio sensitivity of IDT. Continuing the previous study, Xu et al. [10] studied ignition in an *n*-heptane spray in lean methanol/air mixture at three ambient temperatures focusing on NO<sub>x</sub> and soot emissions. No sensitivity to ambient autoignition was noted at high ambient temperatures, unlike in Karimkashi et al. [8] for *n*-dodecane/methanol mixtures.

Regarding previous numerical simulations on methanol ignition, an attempt has been made to resolve the noted narrow ignition window issue for *n*-dodecane/methanol mixtures. Karimkashi et al. [11] proposed adding hydrogen to the premixed methanol/air mixture. This tri-fuel (TF) ignition idea was tested in a series of 0D homogeneous reactor simulations. It was observed that adding hydrogen promotes ignition in *n*-dodecane/methanol mixtures. Surprisingly, adding hydrogen to the lean methane/air ambient was found to retard the ignition. These effects were thoroughly studied using reaction sensitivity analyses wherein the role of hydrogen in promoting (retarding) IDT in *n*-dodecane/methanol (*n*-dodecane/methane) mixtures was elaborated. These 0D results were confirmed by Gadalla et al. [12] in LES of TF combustion for *n*-dodecane ignited premixed methanol/hydrogen blends. It was concluded that adding hydrogen to the methanol/air ambient mixture can smoothen and extend the ignition window of the diesel pilot spray, i.e., less probability for cycle-to-cycle variations in engines. It should be noted that most previous methanol-related studies have not considered the injection of methanol and thus methanol sprays. In the present study, we aim to analyze if the above temperature sensitivity can also be relevant to methanol spray combustion.

Concerning previous engine-related studies on methanol combustion, Dong et al. [13] used a special two-injector cylinder head in a single-cylinder engine with direct injection (DI) of methanol and pilot diesel. They reported high methanol substitution rates (up to 95%) and high indicated efficiency with low NO<sub>x</sub>, CO, and HC emissions. Saccullo et al. [14] used a similar two-injector concept, reporting low emissions and high efficiency compared to injecting only diesel fuel. Li et al. [15] studied a similar two-injector concept using Reynolds-Averaged Navier-Stokes (RANS) and a sector mesh with a 49-species chemical mechanism. The focus of the study was on the methanol spray injection timing effects on the engine process for optimum efficiency and emissions.

Continuing on previous engine-related studies, an attempt has been made to operate methanol DI engines without any pilot diesel. Shamun et al. [16] increased the engine compression ratio ( $\epsilon = 27$ ) to obtain a high-enough temperature for methanol auto-ignition. High engine efficiency was reported, and some issues were noted on flexible engine use due to the very high compression ratio. Related to this approach, Li et al. [17] used methanol DI with a high compression ratio and spark ignition in a RANS-based study. Spray orientation and mixing were noted to be very decisive from the engine operation point of view. Methanol fuel spray experiments in engine-relevant conditions have been conducted by Ainsalo et al. [18], while a single-fuel engine study was performed by Xu et al. [19] comparing methanol DI to iso-octane DI. The benefits of methanol DI over iso-octane DI were noted in engine-out emissions under partially premixed combustion (PPC) operation.

Related to previous numerical investigations on hydrocarbon spray flames, significant effort has been made to understand *n*-dodecane spray combustion better. As pointed out above, ECN Spray A [3] has been a widely used validation case. Some examples of *n*-dodecane Spray A include the study from Pei et al. [20], who compared LES and RANS using DC with a 103-species mechanism. They concluded that the flame lift-off length (FLOL) location should be auto-ignition controlled. Gong et al. [21] conducted LES for Spray A using DC, focusing on the effect of heat release rate on vapor mixing and spreading. Wehrfritz et al. [22] used LES and flamelet-generated manifolds (FGM) for Spray A. Two chemical kinetic mechanisms and different initial O<sub>2</sub> concentrations were compared for the ignition and flame development noting sensitivity to mechanism selection. Kahila et al. [23] made an LES/DC study comparing the effect of pilot spray quantity in a DF setup. The base case was the ECN Spray A, while the pilot injection duration was varied. It was observed that reducing the injection duration had a strong dilution effect. The observed dilution lowers the reactivity of the DF mixture, leading to delayed high-temperature ignition. In summary, there already exists a relatively large amount of data on *n*-dodecane spray flames showing a high level of detail in the predictions.

Based on the above literature review, we note that there is a research gap on high-pressure reacting methanol sprays using LES. In the present work, we continue from our previous non-reacting methanol spray study [24] and aim to fill this knowledge gap by comparing *n*-dodecane and methanol spray flames in engine-relevant conditions using LES, Lagrangian particle tracking (LPT), and direct chemistry (DC). The objectives of the paper are formulated as follows:

1. To validate the LES/direct chemistry model for *n*-dodecane ECN Spray A ( $T = 900$  K,  $P = 6$  MPa)
2. To characterize methanol ignition and lift-off length under modified ECN Spray A conditions
3. To analyze the temperature sensitivity of a methanol spray flame and establish a minimum ambient temperature for a feasible ignition time in engine-relevant conditions
4. To investigate the heat release rate, local equivalence ratio, and the temperature fields and evaluate the difference and similarity between *n*-dodecane and methanol sprays flames at quasi-steady-state.

## 2. Numerical Methods

### 2.1. Gas Phase Governing Equations

The governing equations for the gaseous phase describe the conservation of mass, momentum, energy, and species mass fractions, and they are written as:

$$\frac{\partial \bar{p}}{\partial t} + \frac{\partial \bar{\rho} \tilde{u}_j}{\partial x_j} = \bar{M}_p \quad (1)$$

$$\frac{\partial \bar{\rho} \tilde{u}_i}{\partial t} + \frac{\partial \bar{\rho} \tilde{u}_i \tilde{u}_j}{\partial x_j} = -\frac{\partial}{\partial x_j} (\bar{p} \delta_{ij} - \bar{\rho} \tilde{u}_i \tilde{u}_j + \bar{\rho} \tilde{u}_i \tilde{u}_j - \bar{\tau}_{ij}) + \bar{M}_d \quad (2)$$

$$\frac{\partial \bar{\rho} \tilde{h}}{\partial t} + \frac{\partial \bar{\rho} \tilde{u}_j \tilde{h}}{\partial x_j} = \frac{\partial \bar{p}}{\partial t} + \frac{\partial}{\partial x_j} \left( \bar{\rho} \tilde{u}_j \tilde{h} - \bar{\rho} \tilde{u}_j \tilde{h} + \frac{\lambda}{c_p} \frac{\partial \tilde{h}}{\partial x_j} \right) + \bar{M}_h + \bar{w}_h \quad (3)$$

$$\frac{\partial \bar{\rho} \tilde{Y}_k}{\partial t} + \frac{\partial \bar{\rho} \tilde{u}_j \tilde{Y}_k}{\partial x_j} = \frac{\partial}{\partial x_j} \left( \bar{\rho} \tilde{u}_j \tilde{Y}_k - \bar{\rho} \tilde{u}_j \tilde{Y}_k + \bar{\rho} D \frac{\partial \tilde{Y}_k}{\partial x_j} \right) + \bar{M}_Y + \bar{w}_k \quad (4)$$

where  $\bar{\rho}$ ,  $\tilde{u}_i$ ,  $\bar{p}$ ,  $\tilde{Y}_k$ ,  $\tilde{h}$ , and  $\bar{\tau}_{ij}$  denote the filtered density, velocity, pressure, mass fraction of species  $k$ , sensible enthalpy, and viscous stress tensor, respectively. The overbar denotes an unweighted ensemble average, whereas the tilde ( $\tilde{\cdot}$ ) denotes a density-weighted ensemble average. The source terms  $\bar{M}_\rho$ ,  $\bar{M}_a$ ,  $\bar{M}_h$ , and  $\bar{M}_Y$  allow the coupling between liquid and gaseous phases for mass, momentum, energy, and species. A unity Lewis number is assumed for all species, and thus  $D = \lambda/\rho c_p$  with  $D$  denoting the thermal diffusivity,  $c_p$  and  $\lambda$  the heat capacity and the thermal conductivity of the gas mixture, respectively. The reaction rate for the species  $k$  is denoted by  $\bar{w}_k$  and the heat release rate (HRR) in Eq. (3) is formulated as  $\bar{w}_h = \sum \Delta h_{f,k}^0 \bar{w}_k$ , where  $\Delta h_{f,k}^0$  is the enthalpy of formation. Finally, the system of equations is closed by the filtered ideal gas law.

In LES, Eqs. (1) - (4) are spatially filtered, resulting in additional subgrid-scale (sgs) terms from the non-linear part of the equations, and they can be written in the form  $NS(\bar{\rho}, \tilde{u}_i, \dots) = \bar{\tau}_{sgs}$ . The subgrid-scale terms, which require further modeling efforts, account for the interaction between the resolved and the unresolved scales. Additionally, according to the Boussinesq hypothesis, viscosity can be written as  $\mu = \mu_g + \mu_t$ , where  $\mu$  is the total viscosity,  $\mu_g$  is the molecular viscosity obtained from Sutherland's law [25], and  $\mu_t$  is the turbulent viscosity calculated from

$$\mu_t = c_1 \bar{\rho} \Delta \bar{k}_{sgs}^{1/2} \quad (5)$$

In Eq. (5),  $\Delta$  denotes the filter width calculated from the cell volume  $V_{cell}$  as  $\Delta = V_{cell}^{1/3}$ . The present study uses a  $k$ - $l$  model [26] for the subgrid scale where a transport equation for the subgrid-scale turbulent kinetic energy ( $k_{sgs}$ ) is solved according to

$$\frac{\partial \bar{\rho} \tilde{k}_{sgs}}{\partial t} + \frac{\partial \bar{\rho} \tilde{u}_j \tilde{k}_{sgs}}{\partial x_j} = \bar{P} - \bar{\rho} \bar{\epsilon}_{sgs} + \frac{\partial}{\partial x_j} \left( \mu_t \frac{\partial \tilde{k}_{sgs}}{\partial x_j} \right) \quad (6)$$

where  $\bar{P}$  is the production term calculated as

$$\bar{P} = \bar{\tau}_{sgs, ij} \frac{1}{2} \left( \frac{\partial \tilde{u}_i}{\partial x_j} + \frac{\partial \tilde{u}_j}{\partial x_i} \right) \quad (7)$$

And  $\bar{\epsilon}_{sgs}$  is the subgrid-scale dissipation rate of the turbulent kinetic energy

$$\bar{\epsilon}_{sgs} = c_2 \frac{\tilde{k}_{sgs}^{3/2}}{\Delta} \quad (8)$$

Consistent with our previous studies, we use the values  $c_1 = 0.05$  and  $c_2 = 1.0$  herein [24,27]. A second-order accurate flux-limited scheme is used for spatial discretization, while a first-order method is applied for time integration [28]. The pressure-velocity coupling is implemented in the reacting PISO (Pressure Implicit with Splitting of Operator) algorithm. Simulations have been carried out with the Star-CD code version 2020.1.

## 2.2. Droplet Motion

In Lagrangian particle tracking (LPT), the motion of individual droplets is tracked through the computational domain. Here, standard equations of motion are used for computational droplets. Heat and mass transfer between the two phases is modeled according to the standard correlations by Frössling [29] and Ranz and Marshall [30,31]. Previously, for the ECN Spray A, the authors have successfully modeled the dispersed phase [24] for several fuels, including  $n$ -dodecane and

methanol. Similarly, homogeneous initial droplet size distribution is assumed here, i.e., constant-size droplets are introduced to the computational domain as in [12,27,32]. In addition, the modeling of droplet breakup and dispersion is not considered. More details of the present droplet modeling can be found in [24].

## 2.3. Combustion Modeling

Since chemical time scales are much smaller than fluid-dynamical ones, operator-splitting is performed to separate the transport of species and energy from the chemical reactions within a CFD time step [33, 34]. The chemical source terms in Eqs. (3) and (4) are then formulated as the finite difference between the initial value and the ordinary differential equation (ODE) solution, being only first order accurate from the operator splitting point of view [34]. However, the constant time step used in the current LES is 75 ns ( $Co < 0.6$ ), a practical choice between accuracy and long computational times. Nevertheless, it is assumed to ensure a sufficient resolution for the operator splitting throughout the unsteady reacting spray problem. Similar splitting techniques with relatively small time steps have been previously applied in the turbulent combustion context with successful validations against the DNS [35] data. Based on our numerical observations on the ECN Spray A (see Section 4.2), the present setup offers a good agreement with the reference data. Furthermore, an analytical formulation of the ODE system Jacobian is applied while the ODE system is solved by SuperLU decomposition [28].

The effect of turbulence-chemistry interactions (TCI) is considered via first order closure hypothesis, i.e., reaction rate  $\bar{w}_k \approx \hat{w}_k(\tilde{Y}_i, \tilde{T}, \bar{p})$  and no subgrid-scale model is applied for the chemical source terms in Eqs. (3) and (4). The underlying assumption is that within the high-velocity spray, the turbulence levels lead to such intense mixing that the current relatively high mesh resolution and the direct chemistry integration capture the broadened reaction zone chemistry, leading to a sufficient solution to the reacting problem. Previously, Pei et al. [20] applied the same first-order hypothesis in the Spray A LES context and obtained good results with a grid spacing equivalent to the present work. Very recently, a similar approach was used by Morev et al. [36] with encouraging results for reacting Spray A. Furthermore, multiple LES studies using a first-order approach have shown a rather good agreement against experiments [37–40]. The good performance and minor differences concerning other closure models have been attributed to a relatively high grid resolution [37,39,40]. It is also noted that in the present model problem, no premixed flame is present, requiring further modeling efforts.

As a prerequisite for successful LES, the present model configuration should be able to reproduce the experimental IDT data for the ECN Spray A, similarly to our previous study using LES/FGM and LES/DC in the same configuration [22,23]. Such consistency will be shown later on in the paper. However, it is worth noting that the present numerical approach also poses certain potential limitations regarding TCI. The major concern is to achieve a sufficient grid resolution. For example, earlier spray-LES studies with sophisticated combustion models such as transported probability density function (TPDF) and conditional moment closure (CMC) models have been only applied in the spray-LES context with a lower grid resolution compared to the present work (2 - 8  $\times$  the cell size used in this work) [41–43]. The first order closure hypothesis cannot be generally recommended for such resolutions, which is not the case in the present study.

## 2.4. Chemical Mechanism

Here, liquid  $n$ -dodecane and methanol are used as reference fuels in the numerical spray combustion investigations. The chemical mechanism chosen for both fuels is a skeletal mechanism by Frassoldati et al. [44] (96 species and 993 reactions), abbreviated Polimi96 hereafter.

The mechanism has shown good performance in *n*-dodecane ignition problems [44,45] and in the Spray A context [41,45]. Considering methanol, several authors have validated Polimi96 for laminar flame speed and IDT at various pressure levels [11,12,46]. It has also been used in 3D reacting spray studies involving premixed methanol-air mixtures [8,12]. Hence, the mechanism is validated for both *n*-dodecane and methanol and according to the literature, it performs well for both fuels. Thereby, Polimi96 is used in the present study for the simulation cases. In addition, to assess the mechanism sensitivity, the mechanism by Yao et al. [47] (54 species and 269 reactions) is compared with Polimi96 for *n*-dodecane in Appendix A. The Yao mechanism has shown good performance in *n*-dodecane ignition problems [44,47,48] and in the Spray A context [37,41,47,48]. In addition, a recent mechanism by Wang et al. [49] is used for the sensitivity analysis of a two-stage ignition for methanol. This is discussed in Section 4.1.2.

### 3. Computational Setup

The present study uses ECN Spray A as the baseline case. The Spray A experiments have been conducted with *n*-dodecane ( $n - C_{12}H_{26}$ ). Here, a fuel comparison is carried out between *n*-dodecane and methanol. For both fuels, the mixture used here consists of 21%  $O_2$  content in 22.8 kg/m<sup>3</sup> ambient gas density together with 150 MPa injection pressure and 90  $\mu$ m nozzle hole diameter. For the Spray A case (*n*-dodecane), the initial gas temperature is  $T_0 = 900$  K.

For methanol, a modified Spray A case has been used. Two modifications are involved within the Spray A case for methanol: 1) the fuel has been changed from *n*-dodecane to methanol, and 2) the initial gas temperature has been modified to accommodate for the very low cetane number of methanol ( $\sim 3$ ). While the *n*-dodecane spray is validated at  $T_0 = 900$  K, the methanol spray investigations are carried out at higher temperatures such that for one case, IDT is comparable to that for *n*-dodecane and another case has longer IDT while still IDT < 2 ms. Hence, based on this, two initial gas temperatures have been chosen for methanol,  $T_0 = 1100$  K and  $T_0 = 1200$  K. The chosen temperatures for methanol will be discussed in detail in Sections 4.1.1 and 4.4. Details of the operating conditions in the present fuel comparison are given in Table 1. The fuel properties for *n*-dodecane and methanol are presented in Table 2.

The geometry of the computational domain resembles the combustion vessel at Sandia National Laboratories. The geometry of the computational domain is not exactly similar to the experimental geometry. Still, the total volume matches that in the experiments for which the experimental validation data are obtained. The computational domain is shown in Fig. 1.

Close to the nozzle exit, 31  $\mu$ m cells are used in the radial directions, while in the axial direction, cells are 62.5  $\mu$ m long (1:2 aspect ratio). Further away from the nozzle between 14 – 35 mm (110 – 335D), cubical 62.5  $\mu$ m cells are used. The length of the 62.5  $\mu$ m region downstream from the nozzle is selected to capture the ignition event within this re-

**Table 1**  
Spray injection specifications.

	ECN Spray A	Methanol
Injection parameters		
Fuel	$n - C_{12}H_{26}$	CH <sub>3</sub> OH
Nominal nozzle diameter [ $\mu$ m]	90	90
Fuel temperature [K]	363	363
Injection pressure [MPa]	150	150
Ambient conditions		
Temperature [K]	900	1100, 1200
Pressure [MPa]	6	7.1, 7.7
Density [kg/m <sup>3</sup> ]	22.8	22.8
$O_2$ % (molar)	21.0	21.0
$CO_2$ % (molar)	6.1	6.1
$H_2O$ % (molar)	3.6	3.6
$N_2$ % (molar)	69.3	69.3

**Table 2**  
Fuel properties of methanol and *n*-dodecane.

Fuels	<i>n</i> -dodecane	Methanol
Chemical formula	C <sub>12</sub> H <sub>26</sub>	CH <sub>3</sub> OH
Molecular weight [g/mol]	170	32
Density* [kg/m <sup>3</sup> ]	697.5	722.1
Vapor pressure* [Pa]	1233	$2.56 \times 10^5$
Latent heat* [kJ/kg]	325.9	1046.9
Viscosity* [kg/ms]	$5.6 \times 10^{-4}$	$2.4 \times 10^{-4}$
Critical temperature [K]	658	513
Critical pressure [Pa]	$1.82 \times 10^6$	$7.95 \times 10^6$
Stoichiometric mixture fraction [-]	0.0616	0.1340

\* Values are given at  $T=363$  K

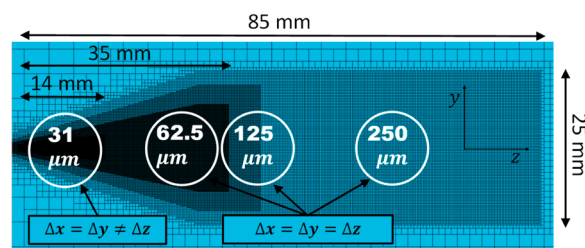


**Fig. 1.** Computational mesh indicating local refinement areas.

gion in all the simulated cases. Starting from 35 mm, 125  $\mu$ m cells have been utilized, followed by 250  $\mu$ m cells between 40 – 85 mm. Such a refinement strategy yields, altogether, 15.5 M cells. The chosen mesh resolution is based on validation studies with different mesh resolutions in the ECN Spray A configuration [21,22]. These studies suggest that close to the nozzle 62.5  $\mu$ m cell size is sufficient for capturing the high gradients and mixing of vapor and the surrounding air. Here, we use 31  $\mu$ m cells near the nozzle to better describe the shear layer dynamics and, consequently, the fuel vapor mixing. In order to see the effect of mesh resolution, a mesh sensitivity analysis is provided in Appendix B.

Below in Fig. 2, a visual illustration of the computational setup is

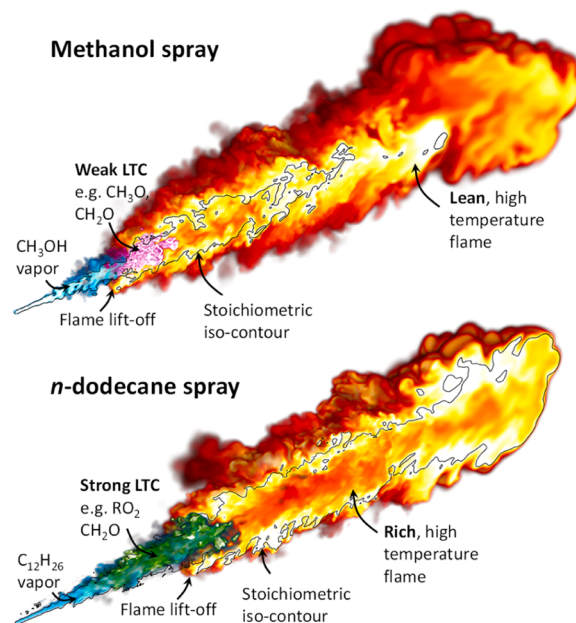


**Fig. 2.** A visual illustration of the computational setup for the *n*-dodecane and methanol spray combustion process. The artwork is based on the authors' numerical work on *n*-dodecane and methanol spray data used to compile the present publication. The 3D volume rendering includes temperature and species concentration (e.g., fuel, CH<sub>2</sub>O) and mixture fraction data.

provided, comparing *n*-dodecane and methanol spray flames. Some general stages are noted on a spray flame development: 1) liquid fuel injection, vaporization, and mixing, 2) volumetric activation of low-temperature chemistry (LTC), i.e., first-stage ignition ( $\tau_1$ ), 3) volumetric activation of high-temperature chemistry (HTC), i.e., second stage ignition ( $\tau_2$ ), and 4) non-premixed flame development. Details concerning the *n*-dodecane spray flame illustration are in line with the presented literature in Section 1, such as strong LTC [41,50] connected to a cool flame prior to FLOL, i.e., activation of species such as  $\text{RO}_2$  and  $\text{CH}_2\text{O}$ , and also increased heat release rate (HRR) before the HTC activation. In addition, generally rich combustion conditions are prevailing for *n*-dodecane spray flames [20,37].

## 4. Results

### 4.1. OD View on Ignition

Here, we analyze the ignition process of homogeneous mixtures, simulated under a OD constant volume homogeneous reactor configuration with an open-source library Cantera [51]. The simulations are performed for *n*-dodecane and methanol using the Polimi96 mechanism discussed in Section 2.4. First, we analyze the high-temperature ignition ( $\tau_2$ ) process for both fuels in Section 4.1.1 and then discuss the possibility of a two-stage ignition event for methanol in Section 4.1.2 below.

#### 4.1.1. High-Temperature Ignition (OD)

We start by analyzing the second stage ignition ( $\tau_2$ ) of homogeneous mixtures of *n*-dodecane and methanol at  $\rho_{\text{gas}} = 22.8 \text{ kg/m}^3$  and for three different equivalence ratios. The chosen density value mimics the ECN Spray A conditions, as discussed in Section 3. First, we examine the ignition delay time (IDT) between the temperature interval 900 K to 1200 K, while allowing pressure to change. Here, IDT is defined based on the maximum pressure gradient. It is noted that using the maximum temperature gradient instead would not change the results appreciably.

Considering the results in Fig. 3, the Spray A case with initial temperature ( $T_0 = 900 \text{ K}$ ) indicates fast ignition for *n*-dodecane while for methanol, this temperature is too low concerning engine relevant time scales (IDT < 2 ms). However, the IDT trend, especially for methanol, is strongly non-linear. In fact, at higher temperatures, e.g., above  $T \geq 1100 \text{ K}$ , methanol IDT is lower than *n*-dodecane IDT. Thus, as an initial guess, Fig. 3 suggests that for methanol, the initial temperature should be at least  $\sim 1050 \text{ K}$  for an IDT comparable or lower than that for *n*-dodecane.

In Fig. 4(a), we consider the mixing line concept, i.e., assuming that the temperatures for the fuel/air mixture is a function of mixture fraction [21], and accordingly plot the IDT as a function of mixture fraction. This trend can be related to the most reactive mixture fraction ( $Z_{MR}$ )

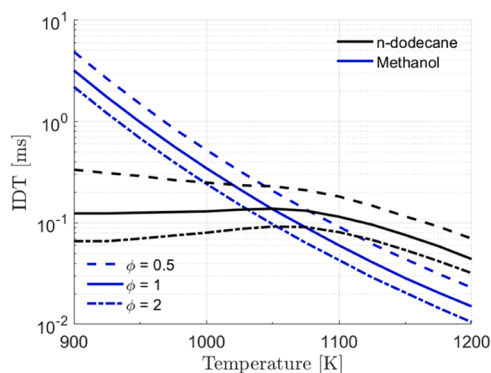


Fig. 3. Ignition delay time (IDT) from OD constant volume homogeneous reactor simulations for methanol and *n*-dodecane for  $\rho_{\text{gas}} = 22.8 \text{ kg/m}^3$  at different equivalence ratios ( $\phi$ ).

concept [52], which describes how the auto-ignition chemistry may prefer a particular mixture fraction, different from the stoichiometric conditions. For example, the early reaction products close to the stoichiometric conditions can be transported to rich mixtures, promoting low-temperature reactions therein [53]. The aim is to find conditions for fast enough ignition considering engine-relevant time scales (IDT < 2 ms). Now for this purpose, we perform OD methanol simulations at two temperatures: 1) Ambient temperature of  $T_0 = 1100 \text{ K}$  and 2) ambient temperature of  $T_0 = 1200 \text{ K}$ . For 1), we expect to see possibly a long IDT below the set 2 ms limit, whereas for 2) we expect fast ignition based on the results in Fig. 3.

For the mixing line concept, the fuel temperature ( $Z=1$ ) is set constant at  $T=363 \text{ K}$  while the ambient mixture temperature ( $Z=0$ ) is  $T_0 = 900 \text{ K}$  for *n*-dodecane, and  $T_0 = 1100 \text{ K}$  or  $T_0 = 1200 \text{ K}$  for methanol. Hence, each mixture fraction value will have a different initial temperature. These temperatures are seen in Fig. 4(b) which shows the mixing line temperature as a function of IDT. Initial pressures are 60 bar, 71 bar, and 77 bar for the *n*-dodecane,  $T_0 = 1100 \text{ K}$ , and  $T_0 = 1200 \text{ K}$  methanol cases, respectively. Again, we use a density of  $\rho_{\text{gas}} = 22.8 \text{ kg/m}^3$  for all cases.

It is interesting to note from Fig. 4(a) that the most reactive mixture fraction  $Z_{MR}$  for *n*-dodecane is on the rich side of stoichiometry ( $Z_{MR, n-dod} = 0.0625$ ,  $\phi = 1.02$ ) while it is lean for the methanol cases ( $Z_{MR, 1100 \text{ K}} = 0.0275$ ,  $\phi = 0.18$  and  $Z_{MR, 1200 \text{ K}} = 0.0325$ ,  $\phi = 0.22$ ). Hence, methanol seems to become more reactive at lean conditions, while the opposite is true for *n*-dodecane. It is seen from Fig. 4(b) how the low reactivity of methanol requires higher temperatures for ignition compared to what is available at stoichiometric conditions ( $Z_{st}$ ). Therefore, the methanol IDTs in Fig. 3 are not very relevant since  $Z_{MR}$  is very lean for methanol. The colored dots in Fig. 4 mark the points that will be further analyzed in the next section.

It is noted that HoV is not considered in  $Z_{MR}$ . Hence, it is expected that in 3D simulations the rich regions will have a lower temperature than the mixing line concept. However, since  $Z_{MR}$  is on the lean side for methanol, the effect of evaporative cooling on methanol IDT might be small. It is also noted that turbulent mixing will significantly affect the IDT, as shown in several 3D spray simulations [12,53]. Table 3 records the IDTs from the OD simulations at  $Z_{MR}$ .

#### 4.1.2. Two-Stage Ignition for Methanol (OD)

Two-stage ignition is a well-known phenomenon for many hydrocarbons, as shown by Warnatz et al. [54] and Simmie [55]. This is related to the differences in chemical activity at varying temperatures. For example, LTC is active at low temperatures, while HTC is active at high temperatures. The Negative Temperature Coefficient (NTC) behavior takes place when the IDT of a mixture is shorter than that at a higher temperature. NTC can be observed for *n*-dodecane ignition, especially at the stoichiometric and rich mixtures. However, for methanol ignition, no NTC behavior can be observed, Fig. 3. NTC is related to the two-stage ignition process at moderate temperatures between LTC and HTC. Next, we focus on the monitoring points in Fig. 4(b) and analyze the ignition process in more detail.

Considering the present study, *n*-dodecane is known to have two-stage ignition, as noted by Vasu et al. [56]. This is also seen in Fig. 5 below using the Polimi96 mechanism, where two conditions have been selected: one for the most reactive mixture fraction ( $Z_{MR}$ ) and one for a richer mixture. The selected points are shown in Fig. 4(b). The points at  $Z_{MR}$  are chosen since the first ignition kernels will appear within this equivalence ratio. Fuel-richer conditions were selected based on the observations by Wang et al. [49]. The  $Z_{MR}$  concept was discussed above in Section 4.1.1.

For methanol, it is reported that no two-stage ignition behavior is observed at low to moderately high pressures, as discussed by Sarathy et al. [57] and Burke et al. [58]. However, recently two-stage ignition for methanol was observed at very high pressures (100 atm) and at rich

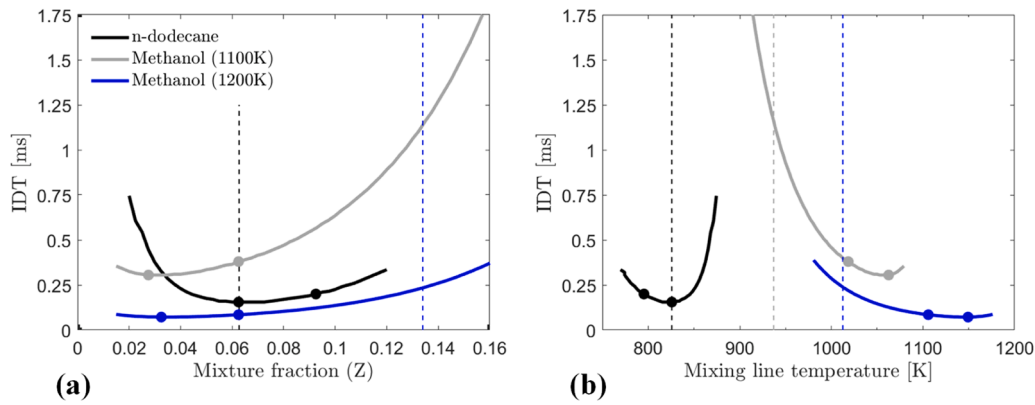


**Fig. 4.** (a) Ignition delay time (IDT) from OD constant volume homogeneous reactor simulations as a function of mixture fraction ( $Z$ ). Vertical dashed lines represent the  $Z_{st}$ . (b) IDT as a function of mixing line temperature. Here, the fuel temperature is constant at  $T = 363$  K while the ambient mixture temperature is  $T_0 = 900$  K for  $n$ -dodecane, and  $T_0 = 1100$  K or  $T_0 = 1200$  K for methanol. Vertical dashed lines represent the corresponding  $T$  at  $Z_{st}$  for  $n$ -dodecane (black), and for methanol 1100 K (gray) and methanol 1200 K (blue). The colored dots are the monitoring points for Section 4.1.2.

**Table 3**

Ignition delay times and flame lift-off lengths (FLOL) from the simulated cases. While the  $n$ -dodecane spray is validated at  $T_0 = 900$  K, the methanol spray investigations are carried out at higher temperatures such that for one case  $\tau_{2,LES}$  is comparable to that for  $n$ -dodecane and another case has longer  $\tau_{2,LES}$  while still  $\tau_{2,LES} < 2$  ms.

	$\tau_{1,LES}$ [ms]	$\tau_{2,MR}^*$ [ms]	$\tau_{2,LES}$ [ms]	$\tau_{2,Exp}$ [ms]	$\tau_{2,LES}/\tau_{2,MR}^*$ [-]	FLOL <sub>LES</sub> [mm]	FLOL <sub>Exp</sub> [mm]
$n$ -dodecane ( $T_0 = 900$ K)	0.072	0.1550	0.302	0.316** / 0.27***	1.95	11.9	12.61** / 9.9***
Methanol ( $T_0 = 1100$ K)	0.600	0.3050	1.276	-	4.18	25.4	-
Methanol ( $T_0 = 1200$ K)	0.075	0.0720	0.240	-	3.33	9.87	-

\* OD result using  $\Phi = 1$ , \*\* CMT experiments [61], \*\*\* Sandia experiments [62].

conditions by Wang et al. [49]. Here, we simulated methanol ignition at high pressures and temperatures. As discussed above, one point of interest was the equivalence ratio at  $Z_{MR}$  while the other chosen point was at somewhat richer conditions. It is noted here that both chosen equivalence ratio conditions for methanol are very lean.

Considering the results from OD homogeneous reactor simulations in Fig. 5, it is interesting that for both initial temperatures ( $T_0 = 1100$  K and  $T_0 = 1200$  K), a two-stage methanol ignition is observed in the mixture of  $Z_{MR}$ , which is similar to that in [49]. However, only single-stage ignition is observed in the slightly richer mixtures ( $Z =$

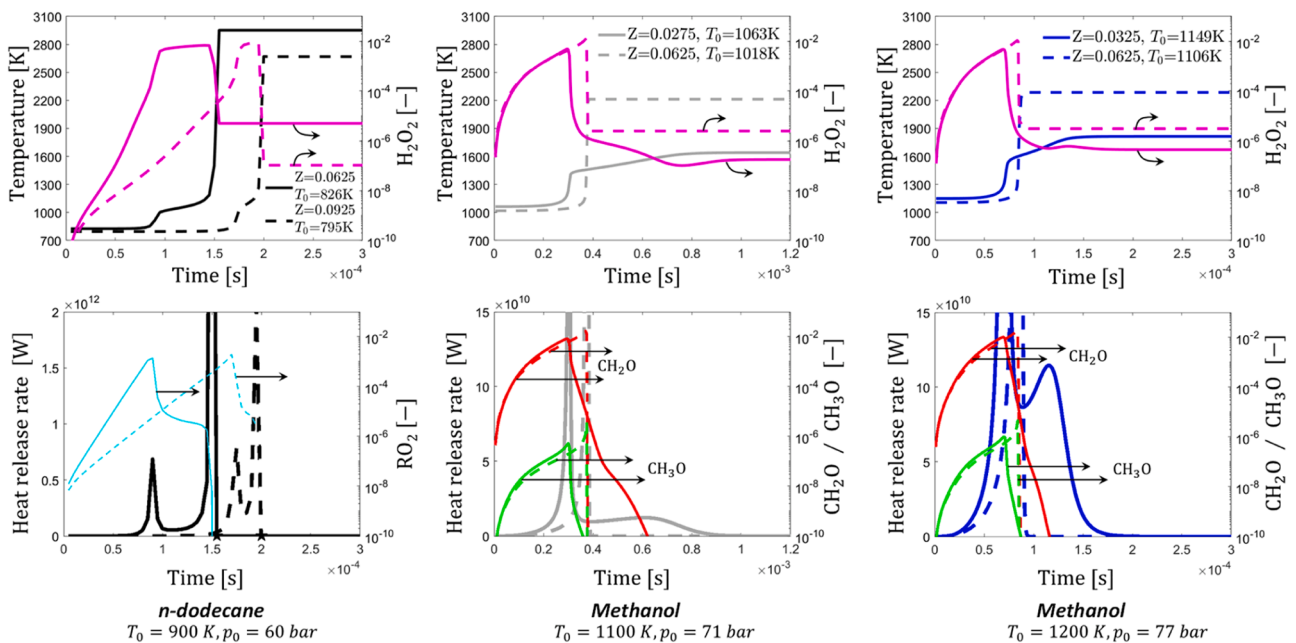


**Fig. 5.** Temperature and  $H_2O_2$  evolution (top row), and heat release rate and  $RO_2$  (light blue) /  $CH_2O$  (red) /  $CH_3O$  (green) evolution (bottom row) in OD homogeneous reactor simulations for  $\rho_{gas} = 22.8$  kg/m<sup>3</sup> using the Polimi96 mechanism. The solid line depicts the conditions at  $Z_{MR}$  while the dashed line shows the situation at richer conditions. The mixture fraction and initial temperature for each case is shown in the legend. The initial pressures are 60 bar, 71 bar, and 77 bar for the  $n$ -dodecane,  $T_0 = 1100$  K, and  $T_0 = 1200$  K methanol cases, respectively. The cases are selected from Fig. 4.

0.0625). This contrasts with that in [49], where two-stage ignition is observed in fuel-rich mixtures. Specifically, we observe a clear accumulation of  $\text{H}_2\text{O}_2$  before high-temperature ignition ( $\tau_2$ ). As noted by Law [59],  $\text{H}_2\text{O}_2$  accumulation slows down the ignition process and thus acts as a marker for two-stage ignition. Here, considering the temperature profiles, two-stage ignition for methanol is characterized by an initial high temperature gradient followed by a slower increase in temperature.

From Fig. 5, it is clear that for the *n*-dodecane flames, the  $\text{C}_{12}\text{H}_{25}\text{O}_2$  ( $\text{RO}_2$ ) mass fraction shows a sudden decrease at the *first-stage ignition*, followed by a plateau of  $\text{H}_2\text{O}_2$  until the onset of *second-stage ignition* where  $\text{H}_2\text{O}_2$  shows a sudden decline. Thus,  $\text{RO}_2$  and  $\text{H}_2\text{O}_2$  may be indicators for LTC and HTC of *n*-dodecane ignition, respectively. After HTC,  $\text{RO}_2$  is completely consumed, while  $\text{H}_2\text{O}_2$  remains low but non-negligible. For methanol flames,  $\text{CH}_3\text{O}$  is consumed at the first-stage ignition, whereas  $\text{CH}_2\text{O}$  is completely consumed at the second-stage ignition. Thus,  $\text{CH}_3\text{O}$  and  $\text{CH}_2\text{O}$  may be the indicators for the LTC and HTC of methanol ignition.

It is worth noting that in contrast to the two-stage ignition of *n*-dodecane where the chemical indicators  $\text{RO}_2$  and  $\text{H}_2\text{O}_2$  have peak values at  $\tau_1$  and  $\tau_2$ , respectively, the defined chemical indicators for methanol ignition both have their peak values at  $\tau_1$ . We consider their complete consumption time instance as the indicator for identifying  $\tau_1$  and  $\tau_2$ . This difference is mainly attributed to the stronger HRR during the first-stage ignition for methanol flames compared to the classical two-stage ignition phenomena where HRR at the second-stage ignition is always stronger than that of the first-stage.

Hence, two-stage ignition phenomenon of methanol has significant differences from that of *n*-dodecane.

- First, the heat release rate at the first-stage ignition of methanol is much higher than that at the second-stage ignition, which is the opposite of the *n*-dodecane ignition, cf. Fig. 5. The onset of two-stage ignition in *n*-dodecane occurs in a rather wide range of temperature and equivalence ratios, whereas for methanol it occurs at rather narrow range of temperature and equivalence ratios.
- Second, the second stage of ignition of *n*-dodecane is associated with the  $\text{H}_2\text{O}_2$  decomposition to OH, which triggers the oxidation of intermediate species. In contrast, for methanol, the decomposition of  $\text{H}_2\text{O}_2$  is at the first stage ignition, associated with a heat release rate two orders of magnitude lower than that after the decomposition of  $\text{H}_2\text{O}_2$  in *n*-dodecane ignition. The lower HRR results in incomplete oxidization of intermediate species, e.g.,  $\text{CH}_2\text{O}$ , which requires a second-stage ignition to fully oxidize.

It is acknowledged that there might be sensitivity to the choice of the chemical mechanism in these high-pressure, high-temperature simulations. Hence, methanol ignition was also simulated with the recent mechanism by Wang et al. [49] for the conditions mentioned in Fig. 5. Qualitatively similar results were obtained as compared to the Polimi96 mechanism (not shown for brevity).

We conclude that two-stage ignition was observed for methanol at high pressure, high temperature, and lean conditions. This will be investigated further in the reacting LES simulations.

#### 4.2. Non-Reacting Spray A Validation (3D)

First, the non-reacting LES model is validated in the Spray A conditions using *n*-dodecane as the liquid fuel. The results are shown in Appendix C for brevity. The present numerical results on average liquid penetration are well in line with the experimental data by Pickett et al. [60]. The average liquid length between 0.2 – 1.5 ms is 10.7 mm compared to the average experimental penetration of 10.0 mm. Here, liquid penetration is defined according to the ECN guidelines using a 0.1% liquid volume fraction for the tip penetration. The average vapor penetration is noted to be slightly under-predicted compared to the

experimental data. The vapor jet tip is obtained as the axial location of 0.1% fuel vapor concentration value according to the ECN guidelines. The obtained radial mixture fraction profiles align with measured data given at two distances from the nozzle. The LES result has been first circumferentially averaged and then time averaged between 1.0 – 1.5 ms. Root mean square (RMS) values are also compared to the experimental data with reasonable accuracy. In summary, the non-reacting Spray A validation shows acceptable correspondence with measured data by Pickett et al. [60].

#### 4.3. Reacting Spray A Validation (3D)

Next, we proceed to validate the reacting Spray A case using *n*-dodecane. The conditions for the validation are given in Table 1. We start by considering the ignition delay time (IDT), here marked as  $\tau_2$  for the high-temperature ignition. Fig. 6 compares the present LES to the experimental data, while Table 3 tabulates the obtained values. The experimental IDT ( $\tau_{2, \text{Exp}}$ ) is noted to vary in the range between 0.27 – 0.316 ms [60,61]. The present LES predicts  $\tau_{2, \text{LES}} = 0.302$  ms. Hence the prediction of  $\tau_2$  is considered to be reasonably accurate. Here, high-temperature ignition ( $\tau_2$ ) is defined based on the maximum temperature gradient ( $\max(dT_{\text{max}}(t)/dt)$ ). The definition based on the OH amount would give a rather similar IDT. It is noted that some LES cases have been repeated (not shown for brevity) and the changes in IDT between the realizations have been below 5%. A qualitative view of the igniting Spray A is given in Fig. 7 (a), where the igniting sprays are shown at  $\tau_2$ . The temperature rise in the spray's tip region is also clearly observed.

After the second stage ignition, the non-premixed spray flame stabilizes at a downstream position referred to as the flame lift-off length (FLOL). Again, Fig. 6 depicts the comparison between LES and the available experimental data. The experimentally observed FLOL for Spray A ranges between  $\text{FLOL}_{\text{Exp}} = 9.9 - 12.61$  mm for the two given experimental sets (Table 3). Here, for the present LES, we obtained  $\text{FLOL}_{\text{LES}} = 11.9$  mm. The result is considered to be rather good compared to the experimental data. Quantitatively, FLOL is defined according to the ECN guidelines as the first axial location of the Favre-averaged OH mass fraction reaching 2% of its maximum in the domain. The averaging was carried out azimuthally in space and between 1.0 and 1.5 ms in time. It is noted that the predicted FLOL has less than a 5% variation between 1.0 – 1.5 ms. In addition, some LES cases have been repeated (not shown for brevity) and the changes in FLOL between realizations have been below 5%. A qualitative view of the FLOL can be seen in Fig. 8, which shows the reacting sprays in a quasi-steady-state situation ( $t = 1.5$  ms for *n*-dodecane). The pressure increase in the constant volume chamber is shown in Fig. 6(c). The LES result is somewhat underpredicted while still within the experimental data scatter. It seems like an advancement in the IDT could yield better agreement with the experimental pressure increase.

#### 4.4. Comparison of *n*-dodecane and Methanol Ignition: Time Evolution of Spray Flames (3D)

In the following, we analyze the *n*-dodecane and methanol spray ignition and flame evolution from the 3D LES perspective. In Section 4.1, numerical evidence was provided on methanol, that the ambient temperature should be at least  $\sim 1050$  K to have a lower or comparable IDT to *n*-dodecane. Based on this, we perform two methanol spray simulations: 1) Ambient temperature is  $T_0 = 1100$  K and 2) ambient temperature is  $T_0 = 1200$  K. For 1), we expect to see rather long IDT yet below the set 2 ms limit, whereas for 2) we expect fast ignition based on the analysis in Section 4.1.

Table 3 records the second-stage IDTs of methanol sprays at these two temperatures predicted in the 3D LES. As a result, for the ambient temperature of  $T_0 = 1100$  K, the IDT is long ( $\tau_2 = 1.276$  ms) but still below the 2 ms limit set above. Furthermore, very high-temperature

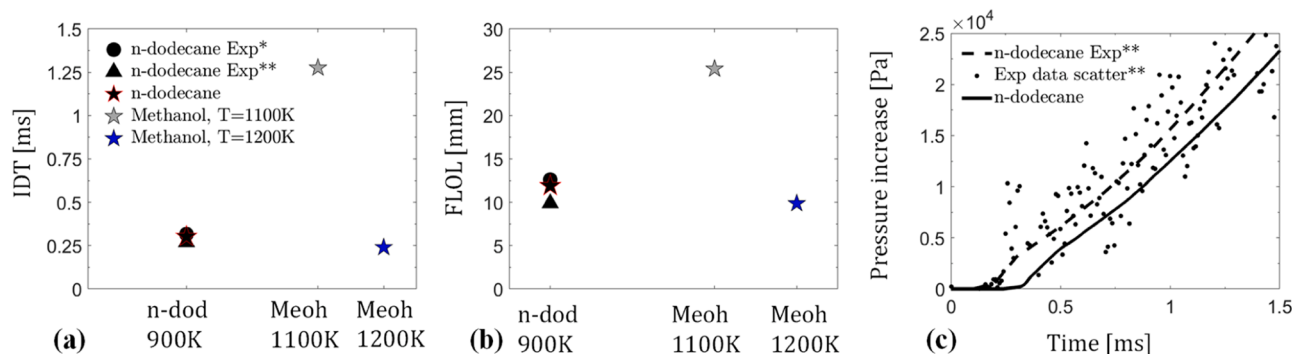


Fig. 6. (a) Ignition delay times (IDT) from the present LES and experiments. (b) Flame lift-off length (FLOL) from the current LES and experiments. (c) The pressure increase in the constant volume chamber from experiments and the present LES. Experimental results are from Benajes et al. [61] \* and from Lillo et al. [62] \*\*.

sensitivity is observed for methanol spray ignition. As  $T_0 = 1200$  K, the IDT is  $\tau_2 = 0.24$  ms, and thus a five-fold decrease in the IDT is observed when  $T_0$  is increased from 1100 K to 1200 K, i.e.  $IDT_{1100\text{K}} / IDT_{1200\text{K}} = 5$ . The effect of mixing is also seen in the ratio of  $\tau_{2\text{LES}} / \tau_{2\text{MR}}^*$ . It is observed that compared to 0D simulations, the IDT in 3D simulations is longer by a factor of 3 – 4. This is attributed to the additional mixing time of the sprays [8].

Qualitatively, Fig. 7 shows the 3D volume rendered ignition event for *n*-dodecane and methanol at  $\tau_2$  and at  $\tau_2 \times 1.25$ . For *n*-dodecane, ignition starts from the spray tip region where the temperature increase is seen. Spatially similar flame structures have been observed in several other studies [20,22,50]. It is interesting to note that for methanol, at both temperatures, ignition takes place axially close to the center of the spray. Considering the equivalence ratio at ignition, *n*-dodecane is igniting from rich regions (see the stoichiometric isoline), which is consistent with previous findings [20,50]. This is also in line with the  $Z_{MR}$  predictions in Fig. 4.

At  $T_0 = 1100$  K, the onset of ignition in methanol spray appears at fuel lean parts of the spray where  $Z < 0.134$ , cf. Fig. 7, consistent with the above  $Z_{MR}$  analysis, although the value is higher than the OD result of  $Z = 0.0275$ . In addition, due to the long IDT, the spray has had a relatively long time to penetrate and mix with the surrounding air. The tip of the  $T_0 = 1100$  K methanol spray has more than twice the penetration compared to the  $T_0 = 1200$  K case (Fig. 7). Ignition for the  $T_0 = 1200$  K case is also taking place axially from the center of the spray. However, based on the provided volume rendering in Fig. 7, ignition starts from the lean region while it is later propagating toward the rich mixture (Fig. 7(b)). Again, the onset of lean mixture ignition is consistent with the  $Z_{MR}$  analysis in Fig. 4.

Next, we will briefly discuss the relevant species related to *n*-dodecane and methanol ignition processes. The onset of the early low-temperature reactions is often referred to as the first-stage ignition (marked here with  $\tau_1$ ), and it includes the production of various intermediate species and radicals. For *n*-dodecane, species such as  $C_{12}H_{25}O_2$  ( $RO_2$ ),  $CH_2O$ , and  $H_2O_2$  have a key role during LTC [20,50,58]. Here, we define  $\tau_1$  as the time instance when 20% of the maximum  $RO_2$  mass fraction is reached in the system for *n*-dodecane. Qualitatively,  $RO_2$  is observed in the first-stage ignition process, cumulating during the first-stage ignition delay time (as indicated in Fig. 5). Once higher temperatures are locally reached at  $\tau_2$ ,  $RO_2$  is completely depleted. The evolution of the maximum  $RO_2$  amount within the spray is displayed in Fig. 9. For methanol ( $CH_3OH$ ) oxidation, the first oxidation products are species such as  $CH_3O$ ,  $CH_2OH$ , and  $CH_2O$  [57]. Qualitatively, Fig. 8 shows that  $CH_2O$  appears axially later, preferring higher temperature conditions than  $RO_2$  for *n*-dodecane ignition. Close to FLOL, e.g.  $CH_2O$  and  $H_2O_2$  have their peak values, while downstream from FLOL, they are quickly oxidized.

#### 4.4.1. Quasi-Steady-State Flame (3D)

Here, we discuss the characteristics of the spray flames at a quasi-steady-state. In this state, the spray flame development is statistically stationary in terms of parameters such as liquid length, FLOL, maximum temperature, and the peak values of several detected combustion products (e.g., OH,  $RO_2$ , or  $CH_2O$ ). Hence, the main temporal change would be related to the reacting spray tip penetration.

Considering the FLOL of the *n*-dodecane spray, we noted in Section 4.3 that it was reasonably predicted compared to the experimental observations. One can have a qualitative view of the FLOL in Fig. 8 where 3D volume rendering of the reacting sprays is shown at the quasi-steady-state. As stated earlier, FLOL is defined based on spatial and temporal averaging of the OH field. However, the OH field is strongly linked to the temperature field shown in Fig. 9. In line with the observations in Section 4.4,  $RO_2$  formation starts close to the nozzle, and is locally depleted once the high-temperature region is reached. Hence, at the FLOL location,  $RO_2$  is consumed. As pointed out in several studies [20,37], FLOL is connected to mixture auto-ignition, i.e., once the radical and temperature buildup within the cool flame region is sufficient, local auto-ignition kernels are formed that end up in the high-temperature flame and in a stabilized FLOL.

For the methanol sprays, the  $T_0 = 1100$  K case shows a high concentration of  $CH_2O$  cumulating around and before the FLOL region. Table 3 shows the recorded FLOL data for the methanol cases. As observed above in Section 4.4, the FLOL location is entirely on the lean mixture region, visible also from Fig. 8. This is connected to the above-mentioned overleaning of the fuel-air mixture resulting in completely lean combustion. Related to this, the FLOL location has been stabilized at a relatively long distance from the nozzle at  $FLOL = 25.4$  mm. The situation looks very different for the  $T_0 = 1200$  K case where more active LTC shows a higher concentration of  $CH_2O$  close to the FLOL region being now low at 9.9 mm. Hence, for the FLOL of the methanol sprays, we obtain  $FLOL_{1100\text{K}} / FLOL_{1200\text{K}} = 2.6$ .

Looking at the  $CH_2O$  concentration of the  $T_0 = 1200$  K methanol case, it is located in a much more confined but higher-temperature region compared to the  $RO_2$  concentration for *n*-dodecane. In addition, some of the high-temperature reactions for the  $T_0 = 1200$  K case are now taking place in the rich mixture, opposite to the  $T_0 = 1100$  K methanol case. For the  $T_0 = 1100$  K case,  $CH_2O$  is located completely in the lean mixture. However, the rich region is much shorter and narrower than the *n*-dodecane flame.

Regarding the local temperatures, the *n*-dodecane flame has a high temperature that seems localized around the stoichiometric mixture. Interestingly, we see a lower temperature region at the core of the spray (downstream of FLOL). Looking at the  $T_0 = 1100$  K methanol spray, the local temperature close to the outer spray boundary is rather low at around  $\sim 1600$  K while the core of the flame, especially close to FLOL, is at a much higher temperature  $T > 2200$  K. Comparing the situation to the  $T_0 = 1200$  K methanol case, high temperatures are observed

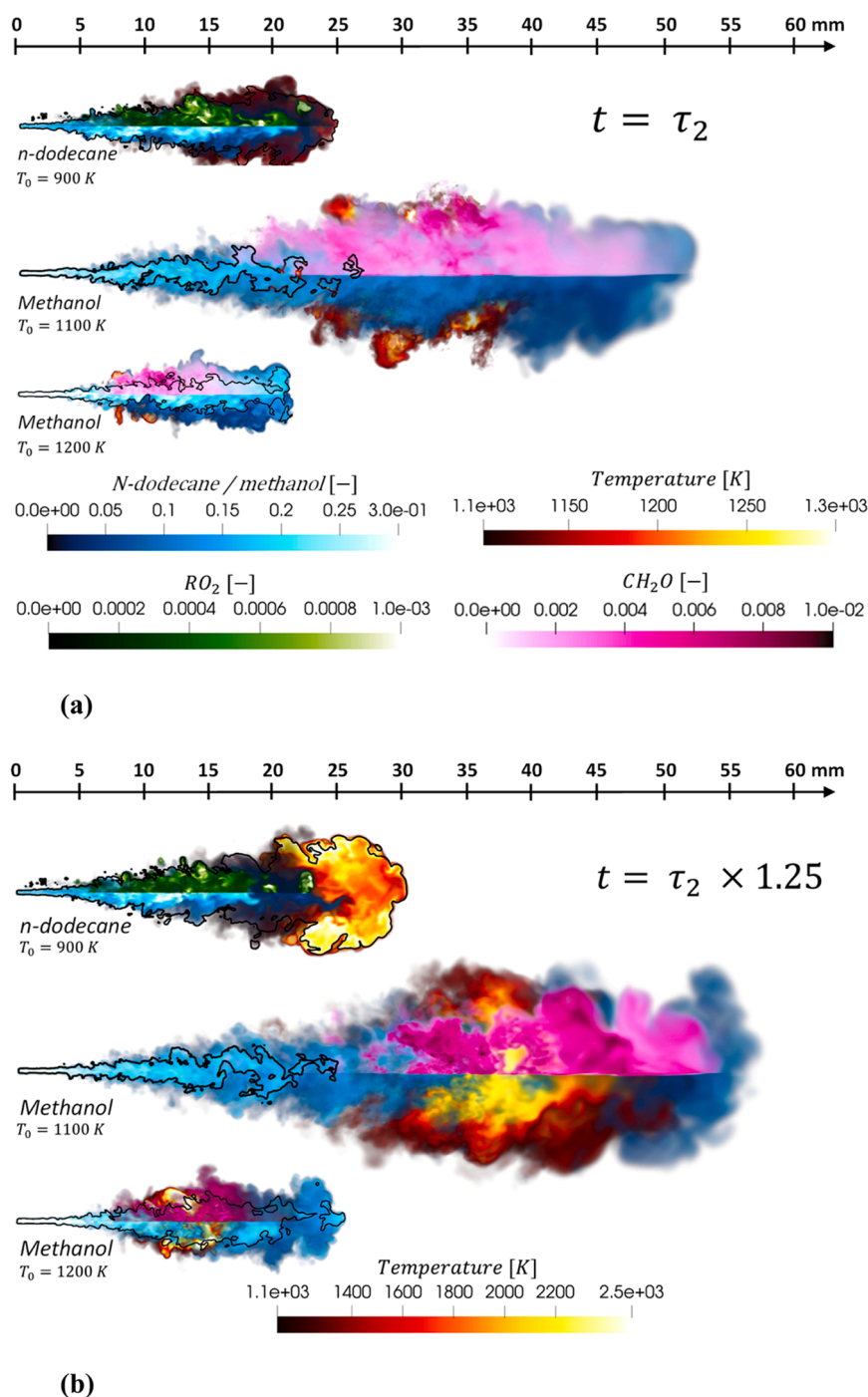


**Fig. 7.** 3D volume rendering of the reacting sprays (cut in half) (a) at time  $\tau_2$  and (b) at time  $\tau_2 \times 1.25$ . The black solid line represents the stoichiometric mixture fraction. Note that similar color scales are used in (a) and (b) except for temperature. For  $RO_2$  and  $CH_2O$ , only top half is shown for improved clarity of view.

primarily close to the stoichiometric mixture. However, because the stoichiometric region is narrow, the high-temperature region is also located at the spray's core, not at the outer periphery as in the *n*-dodecane case. Thereby, the outer edge of the methanol spray flame is cooler than the *n*-dodecane spray flame due to the leaner mixture.

In summary, we note strong temperature sensitivity on methanol FLOL between  $T_0 = 1100$  K and  $T_0 = 1200$  K cases. In addition, very different equivalence ratio fields are observed in the methanol sprays compared to the *n*-dodecane spray. Qualitatively similar FLOL sensitivity has been observed for *n*-dodecane FLOL between temperatures 750 K and 900 K [3]. Quantitative analysis of the reacting spray temperatures and key species is offered in the next Section 4.5.

#### 4.5. Temperature, Species, and Mixture Stratification

We investigate the temperature, species, and mixture evolution for *n*-dodecane and methanol sprays in the following. First, we consider the temperature and species evolution in Fig. 9. The maximum temperature for the *n*-dodecane and  $T_0 = 1200$  K methanol cases is quite similar, with values of 2683 K and 2693 K for *n*-dodecane and methanol, respectively. For the overleaned  $T_0 = 1100$  K methanol case the maximum temperature is lower at 2495 K. Corresponding well with  $\tau_2$ , the OH is increasing simultaneously for all cases. The average ( $Z > 1 \times 10^{-4}$ ) spray temperature at quasi-steady-state is noted to be rather similar between the *n*-dodecane and the  $T_0 = 1200$  K methanol cases,

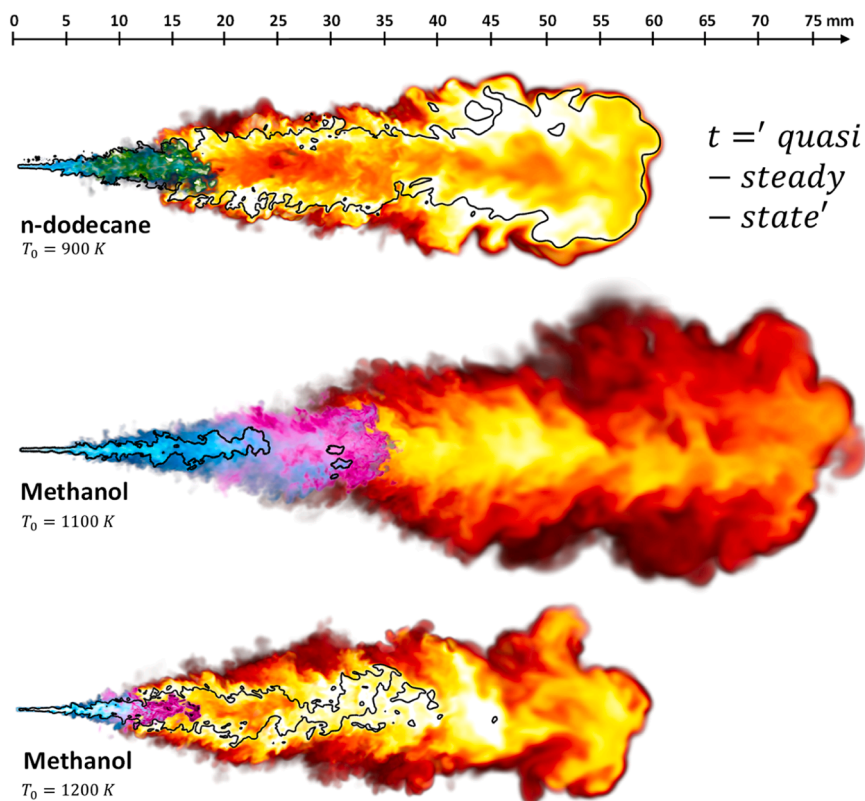


**Fig. 8.** 3D volume rendering of the reacting sprays (cut in half) at quasi-steady-state at  $t = 1.5$  ms for *n*-dodecane and methanol,  $T_0 = 1200$  K, and  $t = 3.0$  ms for methanol,  $T_0 = 1100$  K. The black solid line represents the stoichiometric mixture fraction. Color scales as in Fig. 6 (b).

although the ambient temperature for the methanol case is much higher.

Considering the evolution of key species for *n*-dodecane, Fig. 9 depicts the concentrations of  $\text{RO}_2$ ,  $\text{CH}_2\text{O}$ ,  $\text{H}_2\text{O}_2$ , and OH. The start of slow temperature increase and the cumulation of e.g.  $\text{RO}_2$  and  $\text{H}_2\text{O}_2$  are matching well with  $\tau_1$ . The peak values of these species are seen close to  $\tau_2$ . In physical space, downstream from FLOL,  $\text{RO}_2$  and  $\text{H}_2\text{O}_2$  are quickly oxidized supporting the production of OH.

Analyzing the key species for the methanol sprays, Fig. 9 shows the evolution of  $\text{CH}_2\text{O}$ ,  $\text{CH}_3\text{O}$ ,  $\text{H}_2\text{O}_2$ , and OH. First, there is a temperature increase and cumulation of species such as  $\text{CH}_2\text{O}$  and  $\text{H}_2\text{O}_2$  close to  $\tau_1$ . Especially for the  $T_0 = 1200$  K methanol case, this is followed by a sudden decrease in temperature and chemical activity. Also here, the peak values of these species are seen close to  $\tau_2$ . In physical space, downstream from FLOL, e.g.  $\text{CH}_2\text{O}$  and  $\text{H}_2\text{O}_2$  are oxidized enabling the production of OH. The evolution of  $\text{CH}_3\text{O}$  is seen to peak at  $\tau_2$  while having very low values before that. The temporal evolution of temperature and species in Fig. 9, and the discussion in Section 4.1.2, suggest a two-stage ignition process for *n*-dodecane and methanol.

Next, the temperature evolution at the centerline of the spray is shown in Fig. 10 as a function of time. The cooling effect of methanol is seen especially close to the FLOL (initiation of high temperatures along the  $z$ -axis), where the mixture is cooler for the methanol cases than for the corresponding *n*-dodecane case. The high-temperature core of the methanol sprays is also visible as the centerline temperature for *n*-dodecane is lower than the methanol cases (although the average spray temperature between the *n*-dodecane and methanol  $T_0 = 1200$  K cases is rather similar). The high-temperature ignition timing is also visible here, showing the fast ignition for the methanol  $T_0 = 1200$  K case and the very slow ignition for the methanol  $T_0 = 1100$  K case. The temporal variation of FLOL is also clearly visible.

Finally, we analyze the mixing characteristics of the spray cases, and look at the PDF of the mixture fraction in Fig. 11. We can observe several phenomena taking place for the different cases: 1) The strong leaning of

all the sprays as time progresses. 2) The significant overleaning of the  $T_0 = 1100$  K methanol case, as pointed out also previously. 3) At quasi-steady-state, the lean portion of the mixture is as follows (integrating the mass-based PDFs): 99.5%, 97%, and 69% for the  $T_0 = 1100$  K methanol,  $T_0 = 1200$  K methanol, and *n*-dodecane cases ( $Z > 1 \times 10^{-4}$ ), respectively. On average, the simulated methanol sprays are significantly leaner than *n*-dodecane sprays at quasi-steady-state:  $\phi_{1100\text{meoh, ave}} \approx 0.17$ ,  $\phi_{1200\text{meoh, ave}} \approx 0.25$  vs  $\phi_{ndod, ave} \approx 0.7$ . The lower temperature methanol case has mixed about 5 times longer than the  $T_0 = 1200$  K methanol spray. Hence, the overleaning before ignition leads to an almost completely lean mixture situation. For the *n*-dodecane spray, the rich mixture portion is significant even at quasi-steady-state (31%).

#### 4.6. Heat Release Rate Analysis

Here, we analyze the global and local heat release rate (HRR) between methanol and *n*-dodecane. First, we consider the global HRR and subdivide it into classes based on chemistry (LTC/HTC) and mixture composition (lean/rich). Inspired by recent studies [23,63], we divide the HRR into 5 groups, denoted as LTC, Late LCT, Pre HTC, HTC Pre-ignition, and HTC. The transition between LTC and HTC is not an obvious process. Hence, we set a temperature threshold of 1150K and 1400 K for *n*-dodecane and methanol, respectively, to identify between the two main modes. The sub-division is based on threshold values for  $\text{RO}_2$ ,  $\text{CH}_2\text{O}$ ,  $\text{H}_2\text{O}_2$ , and OH mass fractions, listed in Tables 4 and 5. The threshold values shown here for *n*-dodecane are taken from [23]. Additionally, a hatch pattern is applied for each group to separate rich and lean mixtures.

The optimal threshold values for the HRR mode categorization are acknowledged to depend on the mixture state. The threshold values in Tables 4 and 5 were chosen after carrying out numerical tests on homogeneous OD reactors and transient LES data. Most importantly, the

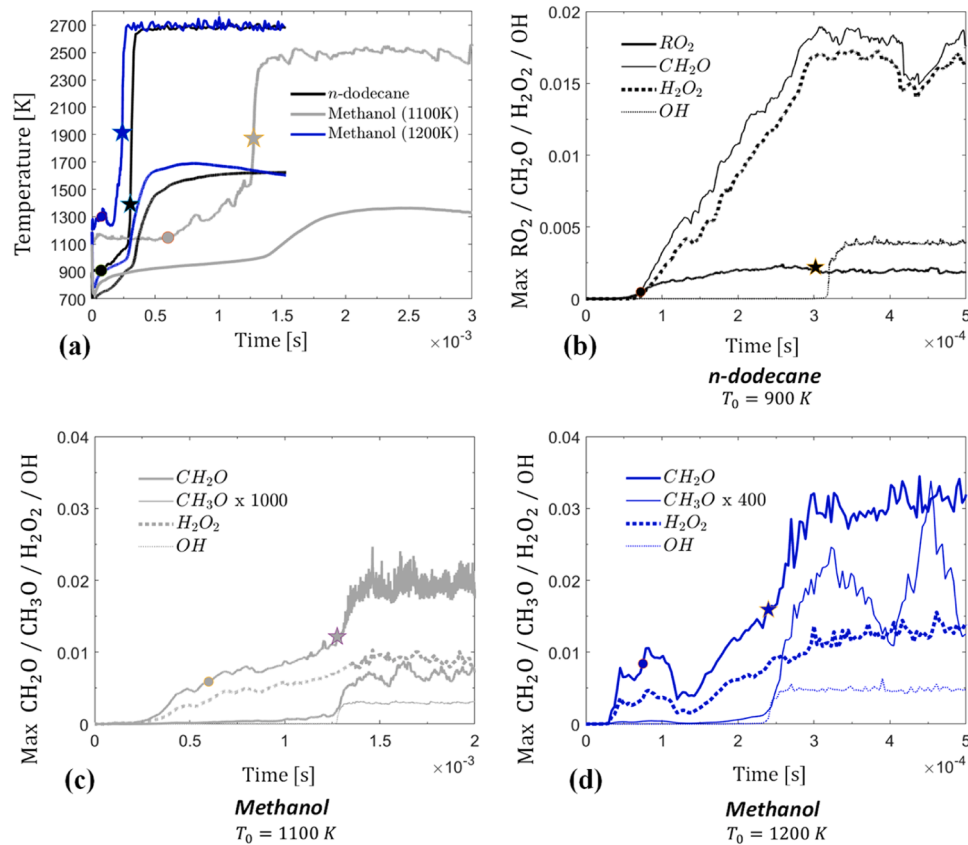


**Fig. 9.** (a) Maximum and average spray plume temperature ( $Z > 1 \times 10^{-4}$ ). Circles mark  $\tau_1$  and stars  $\tau_2$ . (b) Maximum  $RO_2$ ,  $CH_2O$ ,  $H_2O_2$ , and  $OH$  for *n*-dodecane. (c) Maximum  $CH_2O$ ,  $CH_3O$ ,  $H_2O_2$  and  $OH$  for methanol  $T_0 = 1100$  K and (d) for methanol  $T_0 = 1200$  K.

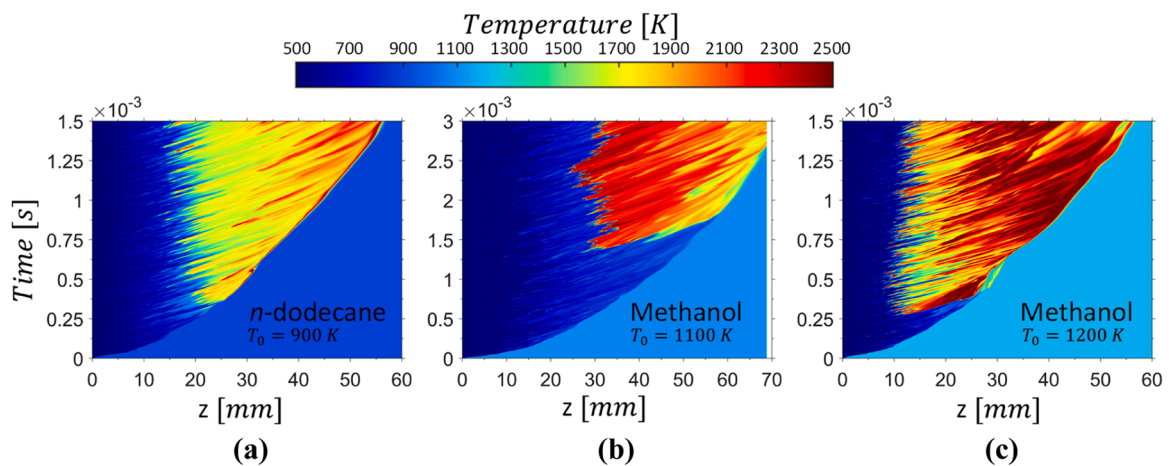


**Fig. 10.** Temperature evolution at the spray centerline ( $z$ -axis) as a function of time. (a) *n*-dodecane,  $T_0 = 900$  K, (b) Methanol,  $T_0 = 1100$  K, and (c) Methanol,  $T_0 = 1200$  K. Note the different scaling in (b). It is observed that while *n*-dodecane ignition occurs at the rich tip region with mild centerline temperature, methanol ignition takes place from the lean spray edge with high spray centerline temperature.

following interpretations made from such a simple categorization were insensitive to the exact threshold values.

Using the above categorization, we can identify different characteristics between the methanol and *n*-dodecane cases based on Fig. 12. 1) It is seen that the  $T_0 = 1200$  K methanol case has weak HRR before  $\tau_2$  while for the  $T_0 = 1100$  K case HRR starts before  $\tau_2$ . 2) For the  $T_0 = 1200$  K methanol case, the start of LTC and HTC are almost synchronized. However, for the *n*-dodecane and the  $T_0 = 1100$  K methanol case, HTC starts later compared to LTC. 3) For *n*-dodecane, 57% of the HRR comes from the rich mixture (based on cumulative HRR). For the  $T_0 =$

1200 K methanol case, 56% comes from a rich mixture while 0% of HRR comes from rich mixture in the  $T_0 = 1100$  K methanol case. 4) *n*-dodecane combustion is a mixture of Late LTC, HTC pre-ignition, and HTC in proportions of 10%, 10%, and 79%, respectively. For the  $T_0 = 1200$  K methanol case, HRR mostly comes from HTC (94%) with a hint from Late LTC (6%). For the  $T_0 = 1100$  K methanol case, a large portion of HRR originates from the Late LTC (45%), while HTC counts for 50% of HRR. 5) After the initial ignition phase (with a premixed HRR peak), the HRR is lower in the methanol cases. This is related to the lower heating value of methanol, roughly 50% of that from *n*-dodecane. In practice (in

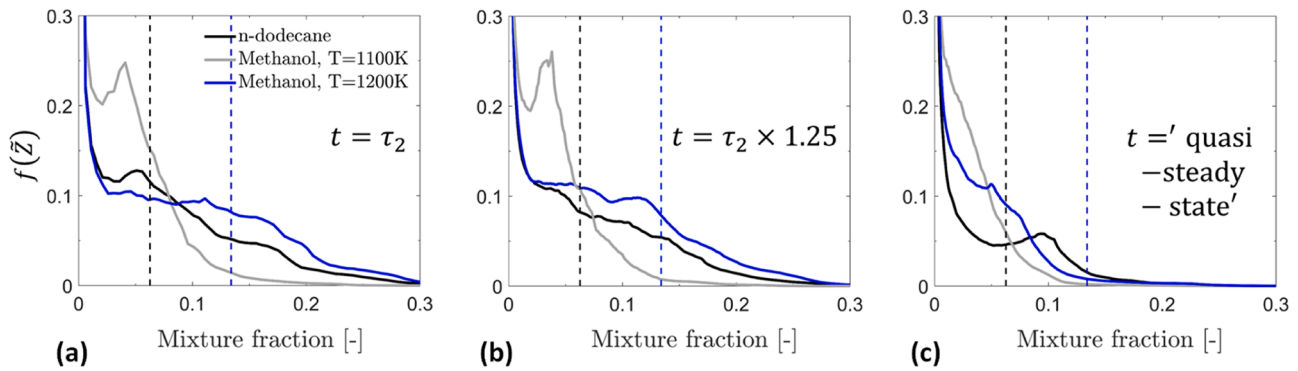


**Fig. 11.** The probability density function of the mixture fraction ( $Z$ ) at time  $t = \tau_2$ , (a), at  $t = \tau_2 \times 1.25$ , (b), and at quasi-steady-state  $t = 1.5$  ms for  $n$ -dodecane and methanol,  $T_0 = 1200$  K, and at  $t = 3.0$  ms for methanol,  $T_0 = 1100$  K (c). Statistics were only considered from the spray cloud ( $Z > 1 \times 10^{-4}$ ). Vertical dashed lines represent the  $Z_{st}$  for  $n$ -dodecane (black) and methanol (blue).

**Table 4**

Grouping of total HRR by chemistry modes for  **$n$ -dodecane**. The critical threshold values are  $T_{cr} = 1150$  K,  $RO_{2,cr} = 1 \times 10^{-5}$ ,  $H_2O_{2,cr} = 1 \times 10^{-4}$ , and  $OH_{cr} = 1 \times 10^{-5}$  (wt%).

Group name	Definition	Fig. 12 color
LTC	$(RO_2 \geq 1 \cdot 10^{-7}) \cap (H_2O_2 < H_2O_{2,cr}) \cap (T < T_{cr})$	
Late LTC	$(RO_2 \geq 1 \cdot 10^{-7}) \cap (H_2O_2 \geq H_2O_{2,cr}) \cap (T < T_{cr})$	
Pre HTC	$(RO_2 < RO_{2,cr}) \cap (H_2O_2 \geq H_2O_{2,cr}) \cap (T < T_{cr})$	
HTC Pre-ign.	$(OH < OH_{cr}) \cap (T \geq T_{cr})$	
HTC	$(OH \geq OH_{cr}) \cap (T \geq T_{cr})$	

**Table 5**

Grouping of total HRR by chemistry modes for **methanol**. The critical threshold values are  $T_{cr} = 1400$  K,  $CH_2O_{cr} = 1 \times 10^{-3}$ ,  $H_2O_{2,cr} = 1 \times 10^{-4}$ , and  $OH_{cr} = 1 \times 10^{-5}$  (wt%).

Group name	Definition	Fig. 12 color
LTC	$(CH_2O \geq 1 \cdot 10^{-6}) \cap (H_2O_2 < H_2O_{2,cr}) \cap (T < T_{cr})$	
Late LTC	$(CH_2O \geq 1 \cdot 10^{-6}) \cap (H_2O_2 \geq H_2O_{2,cr}) \cap (T < T_{cr})$	
Pre HTC	$(CH_2O < CH_3O_{cr}) \cap (H_2O_2 \geq H_2O_{2,cr}) \cap (T < T_{cr})$	
HTC Pre-ign.	$(OH < OH_{cr}) \cap (T \geq T_{cr})$	
HTC	$(OH \geq OH_{cr}) \cap (T \geq T_{cr})$	

an engine application), a higher methanol mass flow rate would be needed compared to  $n$ -dodecane injection.

Here, it is noted that based on the provided HRR plots in Fig. 12, it is difficult to estimate the two-stage ignition phenomena on methanol. This is related to the above mentioned low HRR before  $\tau_2$ . In Fig. 13(a), the computational cell-based maximum HRR is provided as a function of normalized time. It is observed that for  $n$ -dodecane, known to exhibit two-stage ignition, HRR starts to rise after  $\tau_1$ . For the methanol  $T_0 = 1200$  K methanol case, a small rise is seen in the HRR at the time of  $\tau_1$  after which there is a decrease in HRR before  $\tau_2$ . However, for the  $T_0 = 1100$  K case, we see an increase in HRR after  $\tau_1$  in similar fashion to  $n$ -dodecane. It is concluded that together with the observations for the temperature and species evolution in Section 4.4, the 3D LES results

support the OD findings for a two-stage ignition process for methanol at high pressure, temperature and lean conditions.

Next, we will analyze the conditional HRR. In Fig. 13, the HRR is depicted at  $t = \tau_2$ ,  $t = \tau_2 \times 1.25$ , and at quasi-steady-state. Starting from the  $n$ -dodecane ignition event, Fig. 13(b), it takes place in the rich side as pointed out earlier. The HRR for the  $T_0 = 1200$  K methanol case shows an opposite ignition behavior compared to  $n$ -dodecane. That is, even though a rich mixture is available within the spray, ignition takes place from the lean side. It was suggested in Section 4.1 that this is related to the lean  $Z_{MR}$  for methanol. Finally, for the  $T_0 = 1100$  K methanol case, ignition takes place in the lean side of the mixture. In contrast, due to overleaning, the available rich mixture has a low temperature and it is only available close to the nozzle. Low HRR is observed for both methanol cases at ignition.

The conditional HRR at a slightly later instance of time at  $t = \tau_2 \times 1.25$  indicated that, for  $n$ -dodecane, the HRR has moved towards  $Z_{st}$  in mixture fraction space in Fig. 13(c). The HRR for the  $T_0 = 1200$  K methanol case has expanded into the rich mixture region. For the  $T_0 = 1100$  K methanol case, the HRR has moved towards  $Z_{st}$  in mixture fraction space while still entirely within the lean region.

Finally, we investigate the quasi-steady-state local HRR in Fig. 13(d). A distinct double peak in the HRR curve is observed for  $n$ -dodecane. The rich peak reflects the HRR at the FLOL, while the stoichiometric peak comes from the edges of the spray flame. As a remark, at the core of the  $n$ -dodecane spray flame, there is an endothermic (negative HRR) region, reflected by the valley in the Fig. 13(d). However, the HRR magnitude in this region is two orders of magnitude lower than the exothermic HRR. This could be related to the rich core region having a lower equilibrium temperature. The endothermic region is seen as a lower temperature at the core of the  $n$ -dodecane spray (Fig. 8). Similar observation is noted with the Yao mechanism (not shown for brevity). Related to this, lower spray core temperature was also observed in [20] for  $n$ -dodecane. No local endothermic regions were observed for the methanol cases.

Looking at the HRR for methanol sprays at the quasi-steady-state, for the  $T_0 = 1100$  K case, the HRR is entirely on the lean side. For the higher temperature methanol case, the highest HRR is concentrated along the stoichiometry and to the rich FLOL region. However, compared to  $n$ -dodecane, now the stoichiometric mixture region is much narrower at the core of the spray. Thereby, the highest temperature is also closer to the core of the spray compared to  $n$ -dodecane. This effectively cools the edges of methanol sprays, as discussed in Section 4.4.

## 5. Conclusions

In this study, methanol and  $n$ -dodecane spray flames were investigated using LES and DC, along with the Polimi96 mechanism for all cases (96 species and 993 reactions). The aim was to characterize methanol spray combustion and compare it to  $n$ -dodecane spray flames.

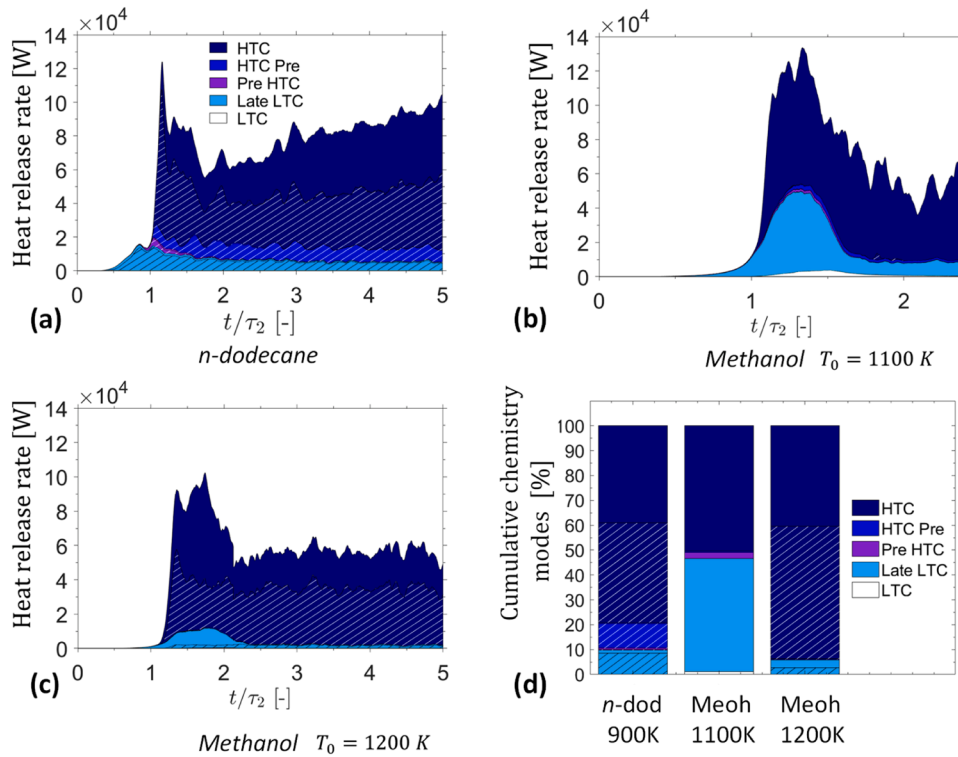


**Fig. 12.** Volume integrated total heat release rate within the spray cloud ( $Z > 1 \times 10^{-4}$ ) as a function of normalized time with a division to classes, defined in Tables 4 and 5. (a) *n*-dodecane, (b) Methanol,  $T_0 = 1100$  K, (c) Methanol,  $T_0 = 1200$  K, and (d) cumulative chemistry modes up to  $t = 1.5$  ms for *n*-dodecane and methanol,  $T_0 = 1200$  K, and up to  $t = 3.0$  ms for methanol,  $T_0 = 1100$  K. Regions with the hatch pattern refer to rich mixtures ( $Z > Z_{st}$ ). Note the different time scales for the methanol,  $T_0 = 1100$  K, case in (b).

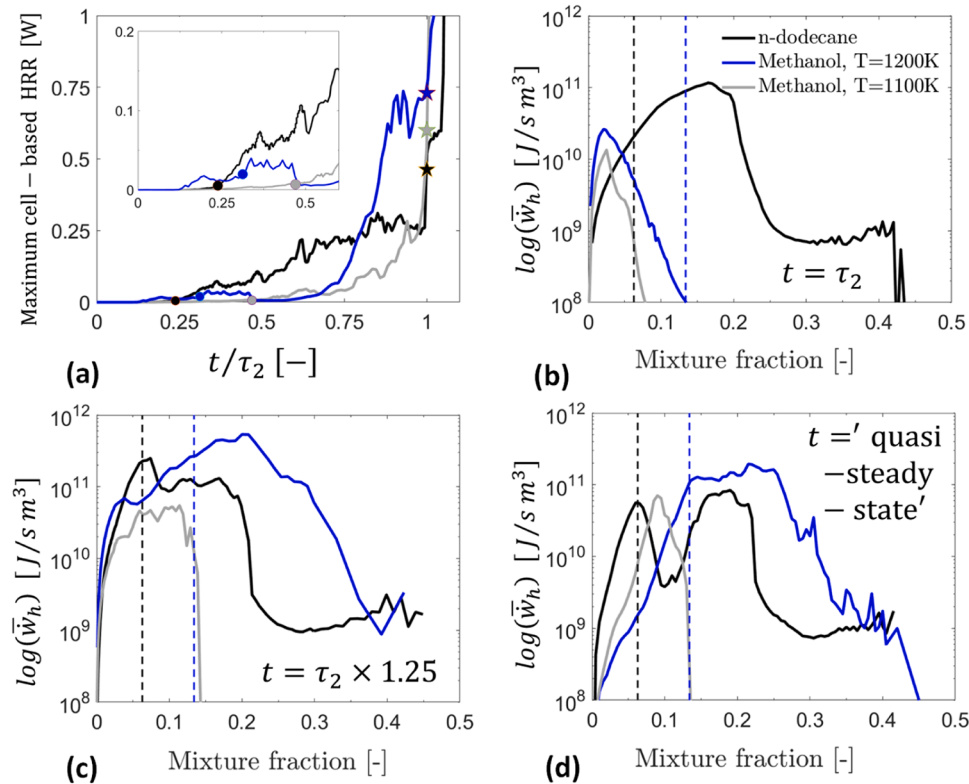


**Fig. 13.** (a) Maximum cell-based heat release rate as a function of normalized time. Circles mark  $\tau_1$  and stars  $\tau_2$ . (b) – (d) Mean (mass averaged) logarithmic HRR values conditioned by mixture fraction at (b)  $t = \tau_2$ , (c)  $t = \tau_2 \times 1.25$ , and (d) at quasi-steady-state  $t = 1.5$  ms for *n*-dodecane and methanol,  $T_0 = 1200$  K, and at  $t = 3.0$  ms for methanol,  $T_0 = 1100$  K. Vertical dashed lines represent the  $Z_{st}$  for *n*-dodecane (black) and methanol (blue).

The LES/DC model was validated for the ECN Spray A under both non-reacting and reacting conditions, and the results showed relatively good performance. The *n*-dodecane case, Spray A, had high ambient pressure (60 bar) and temperature (900 K), along with high injection pressure (1500 bar) and a small nozzle hole diameter (90  $\mu\text{m}$ ). To accommodate the low cetane number of methanol, the nominal Spray A case ambient temperature was modified, and two ambient temperatures (1100 K and 1200 K) were used to achieve an ignition delay time (IDT) below 2 ms. For all simulated cases, the gas density was kept constant at  $\rho = 22.8 \text{ kg/m}^3$ , reflecting the Spray A conditions. Based on the present numerical results, it can be concluded that:

1. The 0D and 3D results both support two-stage ignition characteristics for methanol under lean and high-pressure conditions. This finding is contrary to the typical assumption that methanol does not exhibit two-stage ignition.
2. 3D simulations, supported by 0D reactor cases, indicated a weak HRR and LTC before high-temperature ignition ( $\tau_2$ ) for methanol compared to *n*-dodecane. This is reflected in an almost synchronized initiation of LTC and HTC.
3. In 0D and 3D simulations, strong temperature sensitivity was observed for methanol IDT with a five-fold increase in IDT, i.e.  $IDT_{1100 \text{ K}}/IDT_{1200 \text{ K}} = 5$  (3D LES) and  $IDT_{MR(1100 \text{ K})}/IDT_{MR(1200 \text{ K})} = 4.2$  (0D), as the ambient temperature increased from 1100 K to 1200 K.
4. In both 0D and 3D, methanol sprays ignite first at the fuel-lean mixture, while *n*-dodecane sprays ignite first at the fuel-rich mixture. This is related to the fact that the  $Z_{MR}$  for methanol sprays is smaller than its stoichiometric value. As a result, in 3D LES, methanol sprays ignite axially from the middle of the spray, while *n*-dodecane sprays ignite from the spray tip region.
5. In 3D simulations, the methanol sprays were significantly leaner compared to *n*-dodecane sprays at quasi-steady-state  $\phi_{meoh, ave} \approx 0.2$  vs  $\phi_{ndod, ave} \approx 0.7$ . In addition, 56% of the HRR in the  $T_0 = 1200 \text{ K}$  methanol case originated from the rich mixture, while 0% of the HRR originated from the rich mixture in the  $T_0 = 1100 \text{ K}$  methanol case.
6. In 3D simulations, concerning methanol flame FLOL, strong temperature sensitivity was also predicted for this quantity with 2.6 times longer FLOL when temperature was decreased from 1200 K to 1100 K, i.e.  $FLOL_{1100 \text{ K}}/FLOL_{1200 \text{ K}} = 2.6$ .
7. For 3D LES, depending on the initial conditions, the methanol spray flame may have similar temperatures compared to *n*-dodecane sprays.
8. In 3D simulations, methanol spray ignition exhibits strong sensitivity to the equivalence ratio. The significant temperature sensitivity of the spray ignition may lead to combustion in overlean mixtures, resulting in a low heat release rate due to the overlean mixture. This could lead to low gas temperatures that can potentially contribute to unburned methanol emissions.

The NO<sub>x</sub> emissions from methanol spray combustion in the present study could be evaluated based on the analysis of spray plume

## Appendix A. Mechanism sensitivity

In order to assess the mechanism sensitivity, the mechanism by Yao et al. [48] (54 species and 269 reactions) is compared with Polimi96 for *n*-dodecane. The Yao mechanism has shown good performance in *n*-dodecane ignition problems [44,47,48] and in the Spray A context [37,41,48,49]. The comparison is given in Table A.1 below.

To summarize the comparison, some sensitivity is noted for both first stage ( $\tau_1$ ) and second stage ( $\tau_2$ ). The  $\tau_1$  is predicted to be earlier while the  $\tau_2$  is predicted to be later with Polimi96. This is in line with previous studies e.g. in [37,64]. Concerning the flame lift-off length (FLOL), Yao predicts slightly shorter FLOL compared to Polimi96. However, the prediction of Yao is still within the range of experimental values. In summary, both mechanisms predict the IDT and FLOL for the ECN Spray A (*n*-dodecane) reasonably well. For the rest of the study, all the simulations are performed with the Polimi96 mechanism.

temperatures, bearing in mind that NO<sub>x</sub> formation in such methanol flames is both temperature and chemistry dependant. Accordingly, the emissions may be similar to or lower than those from *n*-dodecane combustion, with a significant dependence on the initial gas phase temperature. The study found a lower total heat release from methanol combustion than from *n*-dodecane combustion, which is related to the lower heating value of methanol. As a practical implication, a greater quantity of methanol may be necessary to compensate for its lower heating value. It should be noted that the present results may be subject to the chosen chemical mechanism and more research on methanol spray flame structure and characteristics is still needed.

## Novelty and Significance Statement

We study high injection pressure (1500 bar) methanol spray flames with LES and finite-rate chemistry, a topic not studied previously. The present homogeneous reactor (0D) and 3D LES simulations revealed a novel phenomenon of a two-stage ignition process for methanol at high pressure, high temperature, and lean conditions. Our results also show that there is a strong ambient temperature sensitivity for methanol IDT and FLOL (five-fold decrease in IDT and a factor of 2.6 decrease in the FLOL when ambient temperature is increased from 1100 K to 1200 K). Furthermore, methanol spray ignition takes place at a very lean mixture contrary to *n*-dodecane ignition and, on average, methanol sprays are significantly leaner than *n*-dodecane sprays. Finally, depending on the initial conditions, methanol spray flames may have similar temperatures as *n*-dodecane sprays, implying comparable levels of NO<sub>x</sub> emissions.

## CRedit authorship contribution statement

**Ossi Tapani Kaario:** Conceptualization, Methodology, Visualization, Writing – original draft, Writing – review & editing. **Shervin Karimkashi:** Investigation, Writing – review & editing. **Atmadeep Bhattacharya:** Investigation, Writing – review & editing. **Ville Vuorinen:** Conceptualization, Writing – review & editing. **Martti Larmi:** Supervision. **Xue-Song Bai:** Conceptualization, Investigation, Writing – review & editing.

## Declaration of Competing Interest

The authors declare that they have no known competing financial interests or personal relationships that could have appeared to influence the work reported in this paper.

## Acknowledgements

The first author acknowledges financial support from the Henry Ford Trust (grant numbers 20220058 and 20230071). This study is also financially supported by the Academy of Finland (grant number 332835) and Aalto University. The authors acknowledge the computational resources provided by the Aalto Science-IT project and Aalto Research Software Engineers (RSEs).

**Table A.1**

Ignition delay times and flame lift-off lengths (FLOL) comparing Polimi96 and Yao mechanisms.

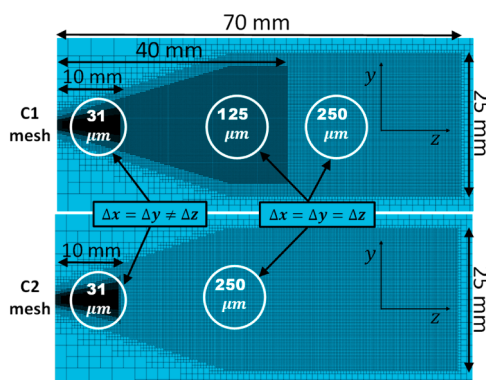
	$\tau_{1, LES}$ [ms]	$\tau_{2, LES}$ [ms]	$\tau_{2, Exp}$ [ms]	FLOL <sub>LES</sub> [mm]	FLOL <sub>Exp</sub> [mm]
<i>n</i> -dodecane (Polimi96)	0.072	0.302	0.316* / 0.27**	11.9	12.61* / 9.9**
<i>n</i> -dodecane (Yao)	0.17	0.270		10.8	

\* CMT experiments [62], \*\* Sandia experiments [63].

**Appendix B. Mesh sensitivity analysis**

In order to see the effect of mesh resolution, a mesh sensitivity analysis was performed. The key strategy is to maintain the near nozzle region at a constant resolution of  $31 \mu\text{m}$  between the dense mesh (Fig. 1) and the coarser meshes shown in Fig. B.1. In this way, the liquid evaporation and the near-nozzle vapor mixing are kept similar between the different mesh resolutions. In addition, we have two coarser meshes compared to the dense mesh. Mesh C1 has  $125 \mu\text{m}$  resolution after the near nozzle region, while the mesh C2 has  $250 \mu\text{m}$  resolution after the near nozzle part. The large reduction of cells is seen in Table B.1 between the cases. Since the near-nozzle region is kept constant between the cases, the time step has also been kept constant at  $7.5 \times 10^{-8}\text{s}$ .

Concerning results shown in Table B.1., the second stage ignition delay time  $\tau_2$  shows some variation compared to the dense mesh (max 15% increase). Considering the variation of  $\tau_2$  in the experiments (max 17%), the variation in the predictions is considered reasonable. In view of the FLOL predictions, some variation is also seen in this quantity around the dense mesh result ( $< 20\%$ ). However, this is in line with the observed experimental FLOL variation (max 27%).

**Fig. B.1.** Mesh sensitivity analysis. The structure of the Mesh C1 and C2.**Table B.1**

Mesh sensitivity analysis.

	Number of cells ( $\times 10^6$ )	$\tau_{2, LES}$ [ms]	$\tau_{2, Exp}$ [ms]	FLOL <sub>LES</sub> [mm]	FLOL <sub>Exp</sub> [mm]
Dense mesh	15.5	0.302	0.316* / 0.27**	11.9	12.61* / 9.9**
C1 mesh	6.1	0.35		10.1	
C2 mesh	3.06	0.30		13.2	

\* CMT experiments [62], \*\* Sandia experiments [63].

**Appendix C. Non-reacting Spray A validation**

The non-reacting LES case for Spray A is compared to experimental data. First, the liquid penetration is compared to experiments in the Fig. C.1. The result is seen to match well with the reference data. The liquid penetration is defined according to the ECN guidelines by using 0.1% liquid volume fraction for the tip penetration. Looking at the vapor penetration, it is observed to be slightly under predicted. Here, vapor jet tip is obtained as the axial location of 0.1% fuel vapor concentration value according to the ECN guidelines. The radial mixture fraction profiles are compared to experiments at two distances from the nozzle in Fig. C.2. The correspondence is observed to be relatively good. In summary, the validation of the non-reacting LES case shows reasonable accuracy against measurements. More information on the non-reacting case can be found from [24].

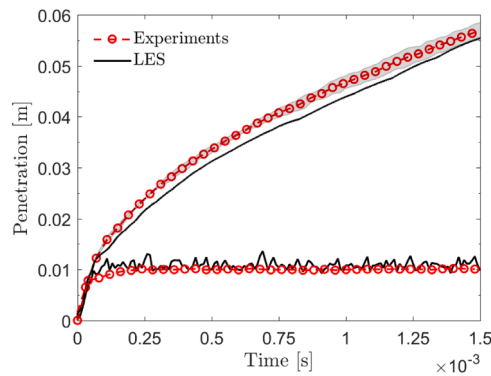


Fig. C.1. Liquid and vapor penetration for non-reacting Spray A with *n*-dodecane.

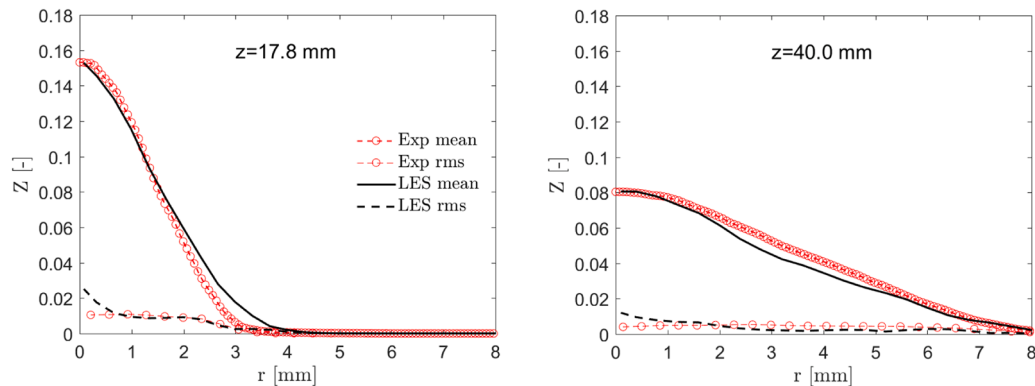


Fig. C.2. Radial vapor profiles at two distances from the nozzle for non-reacting Spray A with *n*-dodecane.

## References

- [1] European commission, Energy systems integration: [https://energy.ec.europa.eu/topics/energy-systems-integration/hydrogen\\_en](https://energy.ec.europa.eu/topics/energy-systems-integration/hydrogen_en).
- [2] S Verhelst, M Turner, L Sileghem, J Vancoillie, Methanol as a fuel for internal combustion engines, *P. Energ. Combust.* 70 (2019) 43–88.
- [3] Engine combustion network workshop 4 (2015).
- [4] F Wang, B Hu, Y Huang, A two-phase turbulent combustion model and its validation for spray flames, *Fuel* 113 (2013) 280–286.
- [5] V Prasad, A Masri, S Navarro-Martinez, K Luo, Investigation of auto-ignition in turbulent methanol spray flames using Large Eddy Simulation, *Combust. Flame* 160 (2013) 2941–2954.
- [6] W Jones, A Marquis, D Noh, An investigation of a turbulent spray flame using Large Eddy Simulation with a stochastic breakup model, *Combust. Flame* 186 (2017) 277–298.
- [7] E Sharma, S De, M Cleary, LES of a lifted methanol spray flame series using the sparse Lagrangian MMC approach, *P. Combust. Inst.* 38 (2021) 3399–3407.
- [8] S Karimkashi, M Gadalla, J Kannan, B Tekgül, O Kaario, V Vuorinen, A Large-eddy simulation of diesel pilot spray ignition in lean methane-air and methanol-air mixtures at different ambient temperatures, *Int. J. Engine Res.* 24 (2023) 965–981.
- [9] S Xu, K Pang, Y Li, A Hadadpour, S Yu, S Zhong, M Jangi, X-S Bai, LES/TPDF investigation of the effects of ambient methanol concentration on pilot fuel ignition characteristics and reaction front structures, *Fuel* 287 (2021), 119502.
- [10] S Xu, S Zong, K Pang, Y Li, S Yu, S Zhong, M Jangi, X-S Bai, Effects of ambient methanol on pollutants formation in dual-fuel spray combustion at varying ambient temperatures: a large-eddy simulation, *Appl. Energ.* 279 (2020), 115774.
- [11] S Karimkashi, H Kahila, O Kaario, M Larmi, V Vuorinen, Numerical Study on tri-fuel combustion: Ignition Properties of hydrogen-enriched methane-diesel and methanol-diesel mixtures, *Int. J. Hydrogen Energ.* 45 (2020) 4946–4962.
- [12] M Gadalla, J Kannan, B Tekgül, S Karimkashi, O Kaario, V Vuorinen, Large-eddy simulation of tri-fuel combustion: diesel spray assisted ignition of methanol-hydrogen blends, *Int. J. Hydrogen Energ.* 46 (2021) 21687–21703.
- [13] Y Dong, O Kaario, H Ghulam, O Ranta, M Larmi, B Johansson, High-Pressure Direct Injection of methanol and pilot diesel: a non-premixed dual-fuel engine concept, *Fuel* 277 (2020), 117932.
- [14] M Saccullo, A Nygren, T Benham, I Denbratt, Alcohol flexible HD single cylinder diesel engine tests with separate dual high pressure direct fuel injection, *Fuel* 294 (2021), 120478.
- [15] Z Li, Y Wang, H Geng, X Zhen, M Liu, S Xu, Parametric study of a diesel engine fueled with directly injected methanol and pilot diesel, *Fuel* 256 (2019), 115882.
- [16] S Shamun, C Hasimoglu, A Murcak, Ö Andersson, M Tuner, Experimental investigation of methanol compression ignition in a high compression ratio HD engine using Box-Behnken design, *Fuel* 209 (2017) 624–633.
- [17] Y Li, X-S Bai, M Tuner, H Im, B Johansson, Investigation on a high-stratified direct injection spark ignition (DISI) engine fueled with methanol under a high compression ratio, *Appl. Therm. Eng.* 148 (2019), 114234.
- [18] A Ainsalo, R Sallinen, O Kaario, M Larmi, Optical investigation of spray characteristics for light fuel oil, kerosene, hexane, methanol, and propane, *Atomization Spray* 29 (2019) 521–544.
- [19] L Xu, M Treacy, Y Zhang, A Aziz, M Tuner, X-S Bai, Comparison of efficiency and emission characteristics in a direct-injection compression ignition engine fuelled with iso-octane and methanol under low temperature combustion conditions, *Appl. Energ.* 312 (2022), 118714.
- [20] Y Pei, S Som, E Pomraning, P Senecal, S Skeen, J Manin, L Pickett, Large eddy simulation of a reacting spray flame with multiple realizations under compression ignition engine conditions, *Combust. Flame* 162 (2015) 4442–4455.
- [21] C Gong, M Jangi, T Lucchini, G D'Errico, X-S Bai, Large Eddy Simulation of air entrainment and mixing in reacting and non-reacting diesel sprays, *Flow Turbul. Combust.* 93 (2014) 385–404.
- [22] A Wehrfritz, O Kaario, V Vuorinen, B Somers, Large Eddy Simulation of *n*-dodecane spray flames using flamelet generated manifolds, *Combust. Flame* 167 (2016) 113–131.
- [23] H. Kahila, O. Kaario, Z. Ahmad, M. Ghaderi Masouleh, B. Tekgul, M. Larmi, V. Vuorinen, A large-eddy simulation study on the influence of diesel pilot spray quantity on methane-air flame initiation, *Combust. Flame* 206 (2019) 506–521.
- [24] O Kaario, V Vuorinen, H Kahila, H Im, M Larmi, The effect of fuel on high velocity evaporating fuel sprays: large-Eddy Simulation of Spray A with various fuels, *Int. J. Engine Res.* 21 (2020) 26–42.
- [25] W. Sutherland, LII. The viscosity of gases and molecular force, *Philos. Magaz. Ser. 5* (36) (1893) 507–531.
- [26] C Speziale, Analytical methods for the development of Reynolds-stress closures in turbulence, *Ann. Rev. Fluid Mech.* 23 (1991) 107–157.
- [27] K Sone, S Menon, Effect of subgrid modeling on the in-cylinder unsteady mixing process in a direct injection engine, *J. Eng. Gas Turb. Power* 125 (2003) 435–443.
- [28] Siemens, Methodology, STAR-CD version 2020.1, (2020).
- [29] Frossling N, Evaporation, heat transfer, and velocity distribution in two-dimensional and rotationally symmetrical laminar boundary-layer flow, Technical Report ADB1891, NACA, (1956).
- [30] W Ranz, W Marshall, Evaporation from drops, part I, *Chem. Eng. Progr.* (1952) 48.
- [31] W Ranz, W Marshall, Evaporation from drops, part II, *Chem. Eng. Progr.* (1952) 48.

- [32] Y. Pei, E Hawkes, S Kook, G Goldin, T Lu, Modelling *n*-dodecane spray and combustion with the transported probability density function method, *Combust. Flame* 162 (2015) 420–435.
- [33] B Sportisse, An analysis of operator splitting techniques in the stiff case, *J. Comput. Phys.* 161 (2000) 140–168.
- [34] Z Lu, H Zhou, S Li, Z Ren, T Lu, C Law, Analysis of operator splitting errors for near-limit flame simulations, *J. Comput. Phys.* 335 (2017) 578–591.
- [35] F Qin, A Shah, Z Huang, L Peng, P Tunestal, X Bai, Detailed numerical simulation of transient mixing and combustion of premixed methane/air mixtures in a pre-chamber/main-chamber system relevant to internal combustion engines, *Combust. Flame* 188 (2018) 357–366.
- [36] I Morev, B Tekgül, M Gadalla, A Shahanaghi, J Kannan, S Karimkashi, O Kaario, V Vuorinen, Fast reactive flow simulations using analytical Jacobian and dynamic load balancing in OpenFOAM, *Phys. Fluids* 34 (2022), 021801.
- [37] H Kahila, A Wehrfritz, O Kaario, V Vuorinen, Large-eddy simulation of dual-fuel ignition: diesel spray injection into a lean methane-air mixture, *Combust. Flame* 199 (2019) 131–151.
- [38] E Hodzic, E Alenius, C Duwig, R Szasz, L Fuchs, A large eddy simulation study of bluff body flame dynamics approaching blow-off, *Combust. Sci. Technol.* 189 (2017) 1107–1137.
- [39] C Duwig, K Nogenmyr, C Chan, M Dunn, Large eddy simulations of a piloted lean premix jet flame using finite-rate chemistry, *Combust. Theor. Model.* 15 (2011) 537–568.
- [40] C Fureby, Comparison of flamelet and finite rate chemistry LES for premixed turbulent combustion, in: 45th AIAA Aerospace Sciences Meeting and Exhibit, 24, American Institute of Aeronautics and Astronautics, 2007. AIAA 2007-1413.
- [41] C Blomberg, L Zeugin, S Pandurangi, M Bolla, K Boulouchos, Y Wright, Modeling split injections of ECN Spray A using a conditional moment closure combustion model with RANS and LES, *SAE, Int. J. Engines* (2016-01-2237) 9 (2016) 2107–2119.
- [42] F Bottone, A Kronenburg, D Gosman, A Marquis, The numerical simulation of diesel spray combustion with LES-CMC, *Flow Turbul. Combust* 89 (2012) 651–673.
- [43] A Irannejad, A Banaeizadeh, F Jaber, Large eddy simulation of turbulent spray combustion, *Combust. Flame* 162 (2015) 431–450.
- [44] A Frassoldati, G D’Errico, T Lucchini, A Stagni, A Cuoci, T Faravelli, A Onorati, R Ranzi, Reduced kinetic mechanisms of diesel fuel surrogate for engine CFD simulations, *Combust. Flame* 162 (2015) 3991–4007.
- [45] J Desantes, J López, J García-Oliver, D López-Pintor, Experimental validation and analysis of seven different chemical kinetic mechanisms for *n*-dodecane using a rapid compression-expansion machine, *Combust. Flame* 182 (2017) 43–57.
- [46] S Karimkashi, H Kahila, O Kaario, M Larmi, V Vuorinen, A numerical study on combustion mode characterization for locally stratified dual-fuel mixtures, *Combust. Flame* 214 (2020) 4946–4962.
- [47] T Yao, Y Pei, B Zhong, S Som, T Lu, K.H. Luo, A compact skeletal mechanism for *n*-dodecane with optimized semi-global low-temperature chemistry for diesel engine simulations, *Fuel* 191 (2017) 339–349.
- [48] Hawkes E, Ignition and flame structure, 5th workshop of the engine combustion network, USA, 2017. Available at [www.sandia.gov/ecn](http://www.sandia.gov/ecn). Accessed Jan. 2018.
- [49] Z Wang, H Zhao, C Yan, Y Lin, A Lele, W Xu, B Rotavera, A Jasper, S Klippenstein, Y Ju, Methanol oxidation up to 100 atm in a supercritical pressure jet-stirred reactor, *P. Combust. Inst.*, In press (2022) 1–9.
- [50] H Kahila, A Wehrfritz, O Kaario, M Masouleh, N Maes, B Somers, V Vuorinen, Large-eddy simulation on the influence of injection pressure in reacting spray A, *Combust. Flame* 191 (2018) 142–159.
- [51] Goodwin D, Speth R, Moffat H, and Weber B. Cantera: an object-oriented software toolkit for chemical kinetics, thermodynamics, and transport processes, <http://www.cantera.org>, version 2.5.1 (2021).
- [52] E Mastorakos, Ignition of turbulent non-premixed flames, *Prog. Energ. Combust.* 3 (2009) 57–97.
- [53] R Dahms, G Paczko, S Skeen, L Pickett, Understanding the ignition mechanism of high-pressure spray flames, *P. Combust. Inst.* 2 (2016) 2615–2623.
- [54] J Warnatz, U Maas, R.W. Dibble, *Combustion*, 2nd edition, Springer, 1999.
- [55] J Simmie, Detailed chemical kinetic models for the combustion of hydrocarbon fuels, *Prog. Energ. Combust.* 29 (2003) 599–634.
- [56] S.S. Vasu, D.F. Davidson, Z Hong, V Vasudevan, R.K. Hanson, *n*-dodecane oxidation at high-pressures: measurements of ignition delay times and OH concentration time-histories, *P. Combust. Inst.* 32 (2009) 173–180.
- [57] S.M. Sarathy, P Obwald, N Hansen, K Kohse-Höinghaus, Alcohol combustion chemistry, *Prog. Energ. Combust.* 44 (2014) 40–102.
- [58] U Burke, W.K. Metcalfe, S.M. Burke, K.A. Heufer, P Dagaut, H.J. Curran, A detailed chemical kinetic modeling, ignition delay time and jet-stirred reactor study of methanol oxidation, *Combust. Flame* 165 (2016) 125–136.
- [59] Chung K. Law, *Combustion Physics*, Cambridge University Press, 2011. ISBN 978-0-521-15421-5.
- [60] L. Pickett, J. Manin, C. Genzale, D. Siebers, M. Musculus, C. Idicheria, Relationship between diesel fuel spray vapor penetration/dispersion and local fuel mixture fraction, *SAE Int. J. Engines* 4 (2011) 764–799.
- [61] J Benajes, R. Payri, M Bardi, P Marti-Aldaravi, Experimental characterization of diesel ignition and lift-off length using a single-hole ECN injector, *Appl. Thermal Eng.* 58 (2013) 554–563.
- [62] Lillo P, Pickett L, Persson H, Andersson Ö, and Kook S, Diesel spray ignition detection and spatial/temporal correction, *SAE Technical Paper* 2012-01-1239 (2012) 1330–1346.
- [63] G Borghesi, A Krisman, T Lu, J.H. Chen, Direct numerical simulation of a temporally evolving air/*n*-dodecane jet at low-temperature diesel-relevant conditions, *Combust. Flame* 195 (2018) 183–202.
- [64] J Kannan, M Gadalla, B Tekgül, S Karimkashi, O Kaario, V Vuorinen, Large eddy simulation of diesel spray-assisted dual-fuel ignition: A comparative study on two *n*-dodecane mechanisms at different ambient temperatures *Int. J. Engine Res.* 22 (2021) 2521–2532.